PICOSECOND LASER PULSES

REPORT K920479-27
SEMI-ANNUAL REPORT

PERIOD COVERED: 1 AUGUST 1970 TO 31 JANUARY 1971

PREPARED UNDER CONTACT N00014-66-C0344
SPONSORED BY
ADVANCED RESEARCH PROJECTS AGENCY ARPA ORDER NO. 306, AMENDMENT NO. 23

United Aircraft Research Laboratories

UNITED AIRCRAFT CORPORATION
EAST HARTFORD, CONNECTICUT 06108

K920479-27

UNITED AIRCRAFT CORPORATION
RESEARCH LABORATORIES
East Hartford, Connecticut

K920479-27
Semiannual Report under Contract N00014-66-C-0344
1 August 1970 to 31 January 197'

ARPA Order No.: 306 Amendment No. 23
Program Cost Code: 000000E0K21
Contractor: United Aircraft Research Laboratories
Effective Date of Contract: 1 August 1966
Contract Expiration Date: 31 Jul, 1971
Amount of Contract: $378,739.00
Contract Number: N00014-66-C-0344
Principal Investigator: Dr. Anthony J. DeMaria (203)565-3545
Scientific Officer: Dr. Robert E. Behringer
Short Title: Picosecond Laser Pulses
Reported by: A. J. DeMaria, W. H. Glenn, G. L. Lamb, Jr., M. E. Mack, E. B. Treacy

Sponsored by Advanced Research Projects Agency
ARPA Order No. 306, Amendment No. 23

Report K920479-27

Semiannual Report Under Contract N00014-66-C-0344
for the Period 1 August 1970 through 31 January 1971

RESEARCH INVESTIGATION OF PICOSECOND LASER PULSES

ARPA Order No. 306, Amendment 23, Project Code No. 000000EOK21

TABLE OF CONTENTS

Security Classification

DOCUMENT CONTROL DATA - R & D

(Security classification of title, body of abstract and indexing annotation must be entered when the overall report is classified)

1. ORIGINATING ACTIVITY (Corporate author)
United Aircraft Corporation
Research Laboratories
East Hartford, Connecituct

2a. REPORT SECURITY CLASSIFICATION
Unclassified

2b. GROUP

3. REPORT TITLE
RESEARCH .NVESTIGATION OF PICOSECOND LASER PULSES

4. DESCRIPTIVE NOTES (Type of report and inclusive dates)
Scientific Se..iannual Report for the Period 1 August 1970 to 31 January 1971

5. AUTHOR(S) (First name, middle initial, last name)
Anthony J. DeMaria, William H. Glenn, George L. Lamb, Jr.,
Michael E. Mack and E. Brian Treacy

6. REPORT DATE	7a. TOTAL NO. OF PAGES	7b. NO. OF REFS
February 25, 1971	79	42

8a. CONTRACT OR GRANT NO.
N00014-66-C-0344

b. PROJECT NO.

c. ARPA Order No. 306, Amendment 23

d. Project Cost Code No. 000000E0K21

9a. ORIGINATOR'S REPORT NUMBER(S)

9b. OTHER REPORT NO(S) (Any other numbers that may be assigned this report)
K920479-27

10. DISTRIBUTION STATEMENT
Reproduction in whole or in part is permitted for any purpose of the United States Government.

11. SUPPLEMENTARY NOTES

12. SPONSORING MILITARY ACTIVITY
Department of the Navy
Office of Naval Research

13. ABSTRACT

This report covers work under contract N00014-66-C-0344 for the period 1 August 1970 to 31 January 1971. Topics discussed include theoretical and experimental work on dynamic spectroscopy of ultrashort light pulses, stimulated scattering effects, nonlinear propagation, organic dye lasers, and flashlamps for organic dye lasers.

DD FORM 1 NOV 68 1473

UNCLASSIFIED
Security Classification

14. KEY WORDS	LINK A		LINK B		LINK C	
	ROLE	WT	ROLE	WT	ROLE	WT
Laser Line Profiles						
Picosecond Laser Pulses						
Ultrashort Pulse Propagation						
Stimulated Scattering						
Organic Dye Lasers						
Mode-Locked Lasers						
Nonlinear Optics						
Dynamic Spectroscopy						

K920479-27

PICOSECOND LASER PULSES

Summary

The effort under this contract during the past reporting period can be divided into four general categories:

1. Dynamic Spectroscopy of Picosecond Pulses: The technical problem involved here is the development of techniques for the measurement of the phase structure of pulses produced by mode-locked neodymium glass (or other) lasers. The work has involved both experimental measurements of the phase structure and analytical modelling of possible phase structure characteristics that are consistent with the experimental results. It has been known for some time that the pulses produced by a mode-locked neodymium glass laser have a time bandwidth product ($\delta\omega\delta t$) that is considerably in excess of the minimum value of approximately 2π that is determined by the classical uncertainty principle. This implies that the pulses do not consist of a smooth envelope modulating a constant optical carrier, but possesses instead an amplitude or phase substructure. Previous works using pulse compression has demonstrated that a considerable portion of the observed bandwidth is due to a sweep of the optical carrier frequency, with lower frequencies preceding the higher frequencies. The information that can be obtained from pulse compression experiments is limited; it would be desirable to obtain a more detailed description of the frequency vs time characteristics of the pulses. The dynamic spectrogram technique that has been developed is capable of providing this more detailed description. A dynamic spectrogram depicts the intensity as a function of frequency and time simultaneously, subject to the uncertainty $\delta\omega\delta t \approx 2\pi$. An instrument for measuring dynamic spectrograms has been developed and demonstrated. This instrument involves the use of an ultrafast spectrometer in conjunction with a two photon absorption cell to display the frequency sweep rate as a function of wavelength for picosecond laser pulses. Measurements have been made that reconfirm the presence of a linear component of the frequency sweep and also indicate the presence of higher order components. Linear, parabolic and sinusoidal dynamic spectrograms (frequency vs time characteristics) have been interpreted theoretically. The change in the dynamic spectrogram of a pulse that is brought about by linear pulse compression and the resultant change in pulse envelope shape have been computed for a typical picosecond pulse.

This work represents an advance in the technology available for the measurement of the detailed properties of optical pulses on extremely short (picosecond) time scales. The techniques developed could be applied to the measurement of the perturbations imposed upon a short pulse by an optical communication channel and to the determination of the ultimate information handling capacity of the channel.

In the area of basic investigations of the interaction of short pulses and matter, the techniques developed provide a valuable tool for the determination of the phase structure changes produced by many linear and nonlinear processes.

2. Pulse Propagation in Resonant Media: The technical problem addressed by the research in this area is that of the nonlinear propagation effects that occur when a short duration pulse propagates in a resonantly amplifying or absorbing media. In this context, a short pulse is meant to imply a pulse of sufficiently short duration compared to the relaxation times of the medium that coherent interaction takes place. Phenomena such as self induced transparency, pulse breakup and photon echoes are examples of such coherent propagation effects. Most of the work in this area at other laboratories has involved numerical computation of the propagation effects; the work under this contract has been analytical and has attempted to obtain closed form solutions describing a number of these effects. This effort has met with a considerable degree of success. Previous work has led to the analytical description of $2n\pi$ pulse propagation. During this period it has been found that the description of the pulse propagation in terms of coupled Maxwell and Bloch equations in the slowly varying envelope approximation shares, with the Korteweg-deVries equation, the property of possessing conservation laws in addition to those of field energy and field momentum. Two conservation laws beyond these have been obtained. They enable one to determine analytically the final amplitude of each of the 2π pulses into which any pulse of area less than 7π will decompose as it propagates through a resonant attenuator.

An article entitled "Analytical Descriptions of Ultrashort Optical Pulse Propagation in a Resonant Medium" by G. L. Lamb, Jr. is scheduled for publication in the April 1971 issue of the Reviews of Modern Physics. This article will present a comprehensive summary of much of the work on coherent pulse propagation that has been supported under the present contract.

The research in this area is of a very fundamental nature. It provides valuable insights into the new types of effects that can occur when high intensity optical pulses interact coherently with matter.

3. Stimulated Raman Scattering and Vibrational Decay Measurements: The work in this area has been concerned with the use of high power picosecond pulses from a mode-locked ruby laser to investigate several aspects of transient stimulated Raman scattering (TSRS) and to make use of TSRS for the investigation of molecular vibrational relaxation times. The work has been mainly experimental. Stimulated Raman scattering requires the buildup of a material excitation. This process has a finite response time determined by the reciprocal of the spontaneous Raman line width. Because of this, Q-switched pulse excitation generally leads to a steady state response while mode-locked pulse excitation leads to a transient response. A number of novel features of TSRS that have been predicted theoretically by other workers have been confirmed experimentally at UARL. It has been verified that: a) the TSRS gain is proportional to the integrated Raman line cross section and is independent of the Raman line width, b) the Stokes pulses are narrowed in time

rather than in frequency as is the case in steady state SRS, c) the Stokes pulses are delayed with respect to the exciting pulse, and d) an estimate can be made of the shape of the exciting laser pulse. Some other important results of the work on TSRS are: a) the observation of strong vibrational SRS in a large number of gases for which SRS had not previously been observed, b) the observation of strong rotational SRS in CO_2, N_2O and O_2; c) the first observation of self focussing in a gas in a parallel beam; and d) the observation of high conversion efficiency that leads to the production of an appreciable molecular population in the excited vibrational state. This makes TSRS important for the investigation of molecular kinetics.

TSRS produces appreciable V = 1 vibrational population in a variety of gases such as N_2, O_2, CO_2, N_2O, CO, HCl, HBr, SF_6, CH_4, C_2H_4 and others. The decay of this population can be monitored by a variety of techniques including: a) subsequent fluorescence (in gases such as CO, CO_2, N_2O, HCl, HBr), b) excited state anti-Stokes scattering using a secondary laser (applicable to all gases), and c) refractive index changes resulting from the thermalization of vibrational excitation (applicable to all gases). These techniques for the measurement of vibrational relaxation times have advantages over other techniques in that measurements can be made at any temperature and that the excitation is highly selective; only the V = 1 state is appreciably populated. Work is currently in progress using techniques a) and c).

The major implication of this work is that TSRS provides a valuable tool for the study of molecular relaxation rates in a number of gases that are of current or potential interest for chemical lasers.

4. Ultrafast Flashlamp and High Power Dye Laser Research: The goal of this program is to develop techniques to obtain reasonably efficient operation and high average power output from organic dye lasers. The work to date has been experimental and has been concerned with the development of several types of flashlamps for use with dye lasers.

An ultrafast capillary tube flashlamp has been developed with a rise time of 10 nsec and a pulse width of 35 - 150 nsec (FWHM). One of the objects of this work was to eliminate the triplet quenching problem that arises when longer duration pulses are used. This type of lamp has been successfully used to excite dyes such as rhodamine 6G and B and sodium fluorescein. These dyes lased strongly and there was no evidence of triplet quenching. The lamps were used in a linear close packed pumping cavity and were operated at an electrical input energy of 2.5 joules. Pulse repetition rates of the order of one per second could be achieved and the overall conversion efficiency (electrical to laser energy) was about 0.04 percent. Maximum optical power output was of the order of one milliwatt. These lamps were used to pump a number of blue-emitting dyes with much less successful results. A number of the normally strongly lasing dyes could not be made to lase. A possible reason for this, and also for the relatively low overall conversion efficiency is the fact that the color temperature of the

discharge is very high (~ 100,000°K). As a result of this, only about two percent of the total emitted energy is in the 2000 - 5000 Å band useful for exciting the visibly emitting dyes. The rich ultraviolet content could lead to population of absorbing excited states which could explain the poor results obtained with the blue emitting dyes.

Another program is in progress to develop a flashlamp capable of handling much higher energies and being operated at higher repetition rates. This lamp is an open arc operated between massive electrodes and at pressures of one atmosphere or above. The rise time of this lamp is longer, of the order of 250 nsec and the total flash duration is of the order of 1200 nsec. The color temperature is lower and consequently a greater fraction (7 - 14 percent) of the energy is emitted in the useful spectral region between 2000 and 5000 Angstroms. The main advantage of this type of lamp is its power handling capability. The energy input per pulse is in the range of 50 - 100 joules and the repetition rates are of the order of 20 pps. The lamp itself has been successfully tested and will soon be used to excite a dye using a specially designed spherical pumping cavity. Estimates of efficiencies based on results of other workers indicate that average laser power outputs in the range of 0.25 - 4 W should be obtainable.

If the performance of this dye laser system meets expectations, it will make available a high average power quasi-continuous source of visible radiation at a very modest cost (compared for instance to a high power, frequency doubled YAG laser). In addition, the output is tunable by a number of techniques that have been used with other dye lasers.

If successful operation is achieved this laser will be a valuable tool for the investigation of a variety of phenomena. Future experiments could involve the production of UV radiation by harmonic generation, the investigation of the frequency dependence of harmonic generation and other nonlinear effects, the investigation of resonant Rayleigh scattering (important for pollution detection) and resonant Raman scattering and experiments on flash photolysis.

Effort supported wholly or in part by the subject contract has led to the following publications and presentations:

a) M. E. Mack, "Bleachable Dyes", presented as an invited paper at the 1970 General Motors Research Conference on the Physics of Opto-Electronic Materials, Warren, Michigan.

b) R. L. Carman, M. E. Mack and J. Reintjes, "Self Trapped Filaments in Gases and Liquids Created from Trains of Picosecond Pulses".

c) R. L. Carman, F. Shimizu, J. Reintjes, N. Bloembergen and M. E. Mack, "Stimulated Raman Scattering in the Picosecond Time Regime".

d) E. B. Treacy, "Pulse Compression and Dynamic Spectroscopy", (Invited Paper). This paper and the preceeding two papers were presented at the 1970 International Quantum Electronics Conference, Kyoto, Japan.

e) G. L. Lamb, Jr. and M. O. Scully, "Higher Conservation Laws for Ultrashort Optical Pulse Propagation in an Inhomogeneously Broadened Medium", presented at the New York Meeting of the American Physical Society, 1-4 February 1971.

f) G. L. Lamb, Jr. "Analytical Descriptions of Ultrashort Optical Pulse Propagation", accepted for Publication in Reviews of Modern Physics, scheduled for April 1971 issue.

g) G. L. Lamb, Jr. "Higher Conservation Laws in Ultrashort Optical Pulse Propagation", Physics Letters 32A, 251-252, 27 July 1970.

h) E. B. Treacy, "Picosecond Light Pulses", Colloquium presented at the Physics Department, University of Queensland, Queensland, Australia, September 25, 1970.

SECTION I

Measurement and Interpretation of Dynamic Spectrograms of Picosecond Light Pulses

This section is a preprint of a paper with the above title by E. B. Treacy that has been submitted for publication in the Journal of Applied Physics.

Physical optics has been concerned primarily with quasi-continuous wave trains, with little effort devoted so far to the study of optical pulses. The present paper describes an attempt to study picosecond pulses[1] generated by a mode-locked Nd:glass laser, using extensions of some well known principles of physical optics for design of instrumentation that can match in time response the rapid time development of the pulse itself.

The important structure measurements made previously on picosecond pulses have been: (i) time resolved spectra[2], which display the spectrum of each member of a section of the pulse train on film; (ii) intensity correlation of pulses through second harmonic generation[3] (SHG) and through two-photon absorption fluorescence[4,1] (TPF); and (iii) combination of pulse compression[5,6] with TPF.

The information obtained from these techniques is in the following forms. Time resolved spectra give $|g(\omega)|^2$ where $g(\omega)$ is the Fourier transform of the pulse $A(t)e^{i\psi(t)}e^{-i\omega_0 t}$, A and ψ denoting the amplitude and phase modulations. The measurements reveal a spectral content of typically 100 cm^{-1} to 200 cm^{-1} in the individual pulses, which is sufficient to yield pulse durations as short as 0.3 psec to 0.15 psec. The intensity correlation techniques give the symmetric function $\int A^2(t)\, A^2(t+\tau)\, dt$, sensitive only to the amplitude structure and not to the phase modulation. The pulse shape cannot be reconstructed from the intensity correlation, although an estimate of the effective pulse duration is readily obtained. It is typically 5 psec to 10 psec, the discrepancy with the subpicosecond numbers quoted above indicating the existence of considerable phase modulation. Pulse compression techniques give $\int B^2(t)\, B^2(t+\tau)dt$ and $\int B^2(t)\, A^2(t+\tau)dt$ where B(t) is the amplitude of a Fresnel transform[7] of $A(t)e^{i\psi(t)}$. The technique depends on introducing a frequency dependent time delay into the pulse to transform it into another pulse in which the amplitude B is sensitive to the original phase modulation ψ. Subpicosecond components are found on the transformed pulses proving that the original pulses have a positive frequency sweep over a considerable portion of their effective duration. The intensity correlation of the compressed pulse against the original pulse reveals an asymmetry in the pulse envelope, the rise time being longer than the fall time.

All the above techniques suffer in being very indirect making it difficult to deduce the AM and FM pulse structure. There are no optical oscilloscopes that

can display a short light pulse in the way that a conventional oscilloscope displays an audio or radio frequency pulse. However, there exists for the audio spectrum a technique that appears to be adaptable to picosecond pulse technology wherein one measures a dynamic spectrogram[8,9] (also called a sonagram) in which the intensity and carrier frequency are displayed as functions of time. The present paper discusses experimental techniques for dynamic spectroscopy of picosecond pulses and the interpretation of some simple spectrograms in terms of amplitude and phase modulation. Since standard high resolution spectroscopy can be performed simultaneously with the dynamic spectroscopy, particular emphasis is placed on measurement of the shape of the spectrogram. A knowledge of the shape of the spectrogram and the spectral amplitude is sufficient in many cases for reconstruction of the optical pulse.

There are circumstances in which a dynamic spectrogram is actually a much simpler representation of pulses than is a description of the AM and FM. The phase structure curve for a hypothetical pulse shown in Fig. 1 which gives a functional relationship between carrier frequency $\dot{\varphi} = \omega_o - \dot{\psi}$ and time t, will be used as an example to illustrate this point. The lower part of the curve depicts a decrease in carrier frequency followed by an increase, thus making the time a double-valued function of the frequency. This effect will lead to a modulation of the power spectrum, with the local periodicity in spectral intensity $I(\omega)$ reflecting the difference between the times at which the carrier frequency passes through the corresponding value of ω. Such effects are well known in optical spectra of short pulses.[10] Obviously one must also consider the possibility of $\dot{\varphi}$ being a multiple-valued function of t as on the left side of the curve of Fig. 1.1. During the time interval that ω is double-valued the upper and lower branches of the curve interfere giving pulsations in the pulse amplitude. At a certain time, $\dot{\varphi}$ can change from double-valued to single-valued so that if one is to represent the pulse by a single expression like $A(t)e^{i\psi(t)}e^{-i\omega_o t}$, the phase term $\psi(t)$ will show a jump in its time derivative at that point, and the pulsations in envelope due to interference between the two branches of $\dot{\varphi}$ will disappear. Even if one could observe an oscillogram of the pulse under discussion, the underlying simple phase structure would be difficult to deduce. For this and other reasons, it makes sense to attempt to measure the dynamic spectrogram, the shape of which resembles the phase structure curve; and then to deduce the corresponding AM and FM.

A chirped pulse will cause sequential responses in a set of bandpass filters tuned to different frequencies. In Fig. 1 the responses at times $\tau_1(\omega_2)$, $\tau_2(\omega_1)$, $\tau_2(\omega_3)$, $\tau_3(\omega_1)$ and $\tau_4(\omega_2)$ are illustrated for filters ω_1, ω_2 and ω_3 each with width $\delta\omega$ and response time δt approximately equal to $2\pi/\delta\omega$. Because of the classical uncertainty between frequency and time measurements it may be convenient to think of the $\omega - \tau$ space as being divided into cells of area 2π by a rectangular grid, and a physical measurement of the type under discussion could at best result in the assignment of a complex number representing the analytic signal to each cell of the space, to yield a kind of matrix as discussed by Gabor.[8,11] For picosecond pulses, our aim at present is less ambitious in

that we seek only the intensities in the various cells. If only a few cells are filled it is more convenient to think of the information as being conveyed in the form of a density in the $\omega - \tau$ plane (as on a photographic plate) with a low resolution, the area of the resolvable spot being roughly the cell size. Within the constraint $\delta\omega\,\delta t \approx 2\pi$, there is still the cell shape to be considered, and some judicial choice could be made if we knew beforehand the shape of the phase structure curve; but in general one should attempt perhaps to divide the total time duration Δt of the pulse and the total bandwidth $\Delta\omega$ into approximately the same number of intervals, this number being roughly the square root of the time-bandwidth product N of the pulse, defined by

$$N = \Delta t(\Delta\omega/2\pi) \tag{1.1}$$

The phase structure curve will then pass through at least $\sqrt{N}$ cells and can thus be determined with this same number of resolvable points.

Thus, one would like to know the phase structure curve, but in fact, by making measurements with filter responses would obtain the dynamic spectrogram† which gives the intensity and carrier frequency (defined to within $\delta\omega$) versus time (defined to within δt). A high resolution spectrometer uses a δt much larger than the pulse duration Δt to present a spectrum $|g(\omega)|^2$ whereas measurement of the pulse AM and FM would require an instrument such as an oscilloscope with $\delta\omega$ much larger than the pulse bandwidth $\Delta\omega$. Denoting the phase of $g(\omega)$ by $\varphi(\omega)$, that is $g(\omega) = |g(\omega)|e^{i\varphi(\omega)}$, it is clear that the spectrometer gives $|g(\omega)|^2$ whereas the dynamic spectrogram sacrifices some information on $|g(\omega)|^2$ to provide partial information on $\varphi(\omega)$.

Interpretation of Simple Spectrograms

If a measured spectrogram has everywhere a width approximately equal to the theoretically expected minimum as determined by the $\omega - \tau$ uncertainty, we call it "simple". Not all pulses are expected to have a simple spectrogram, for example a short burst of random noise might have as its spectrogram an intensity that changes slowly from cell to cell, covering an extended region of the $\omega - \tau$ space. (On the other hand a simple spectrogram may produce an AM that looks much like random noise.)

From the simple spectrogram one reads the arrival time $\tau(\omega)$ at a point in space as a function of angular frequency ω. As a result of the uncertainty one does not know the exact details of the curve τ versus ω, but as a guess might choose to draw the curve smoothly through the most intense part of the spectrogram.

---

† The term "dynamic" (rather than "time-resolved") spectroscopy is preferred when the instrumentation comes close to achieving the minimum uncertainty $\delta\omega\delta t \approx 2\pi$.

This guess will be fairly accurate if the width of the spectrogram is close to its theoretical minimum. If the resulting curve is a vertical straight line, corresponding to identical arrival times τ for all wave groups ω, there is little phase modulation and $g(\omega)$ may be chosen real ($\varphi(\omega) = 0$) with good approximation. (The quality of the approximation does not affect the following considerations.) The corresponding pulse is given by

$$C(t) = \int_{-\infty}^{\infty} g_v(\omega)\, e^{-i\omega t}\, d\omega \tag{1.2a}$$

$$= \int_{-\infty}^{\infty} |g(\omega)|\, e^{-i\omega t}\, d\omega \tag{1.2b}$$

where $g_v(\omega)$ corresponds to the vertical line spectrogram and where the second equality is the approximation.

If $\tau(\omega)$ is single-valued, the pulse could in principle be processed by a linear system (called a pulse compressor) that would make $\tau(\omega)$ independent of ω and Eq. (1.2) would now describe the compressed pulse. The quality of this compressed pulse will be discussed below. The actual pulse $|g(\omega)|e^{i\varphi(\omega)}$ has a spectrogram that may be considered as having been generated by a simple transformation on the pulse described by Eq. (1.2) having $\tau(\omega) = 0$. Any element of the spectrogram at frequency ω has been transformed through a group delay $\tau(\omega)$ from $\tau = 0$ to its present position. This group delay is related to the phase shift $\varphi(\omega)$ by the relation

$$\tau(\omega) = d\phi(\omega)/d\omega \tag{1.3}$$

Integration of Eq. (1.3), therefore, gives the required phase in terms of the measured $\tau(\omega)$:

$$\phi(\omega) = \int^{\omega} \tau(\omega')\, d\omega' \tag{1.4}$$

and the actual time representation of the pulse is given by the Fourier transform:

$$\int_{-\infty}^{\infty} |g_v(\omega)|\, e^{i\int^{\omega}\tau(\omega')d\omega'}\, e^{-i\omega t}\, d\omega = \frac{1}{2\pi}\int \Psi(t')G(t-t')\,dt' \tag{1.5}$$

by the faltung theorem, where G describes the corresponding compressed pulse and

$$\Psi(t) = \int_{\omega_1}^{\omega_2} e^{\,i\int^{\omega}\tau(\omega')d\omega'}\, e^{-i\omega t}\, d\omega \tag{1.6}$$

Here the interval ω_1 to ω_2 has to enclose the range where $|g(\omega)|$ is non-zero. Equation (1.5) gives the actual pulse as a convolution between its compressed counterpart G(t) containing the spectral amplitude information (obtained from a spectrometer), and the function $\Psi(t)$ which contains the phase information (obtained from the spectrogram). In what follows, we shall compute $\Psi(t)$ for some simple single-valued forms of the function $\tau(\omega)$. (If $\tau(\omega)$ is not single-valued, the spectrogram may be divided into segments having single-valued τ, and each segment may be analyzed separately.)

It is at this point that one would prefer to have available Gabor's matrix of complex numbers rather than just the intensities. The relative phases of different filter responses are related simply to the arguments of these complex numbers. (See Fig. 1.9 of Gabor's paper[8].) Consider for example the vertical spectrogram that has been generated by transforming the τ's to have a constant value as just described. If the different filter signals all peak in phase with one another at an instant in the interval spanning the common $\tau(\omega)$, then the pulse being measured is about as short and its peak amplitude as large as its bandwidth and energy will allow, and Eq. (1.2b) will describe the compressed pulse G(t) accurately. If the phases of the filter excitations do not satisfy this ideal condition, the pulse G(t) will be more complex and may be noise-like with total duration somewhere between that of the ideal compressed pulse of Eq. (1.2b) and the width of the spectrogram, depending on the randomness of the phase. Equation (1.5) still holds: it is just that one cannot easily decide the best choice for G(t); but the nature of the convolution is such that the choice of Eq. (1.2b) will be most satisfactory for long pulses, and the error introduced into the pulse waveform calculation will tend to be worst where $\tau(\omega)$ is stationary. Near these stationary points the pulse envelope will be changing slowly anyway, and the approximation will be good wherever the pulsations in intensity are wide compared to δt. In summary, if the measured spectrogram is simple and single-valued in τ, the procedure outlined here for deducing the pulse AM and FM characteristics from the measured spectrum and spectrogram shape (using Eqs. (1.2b), (1.6) and (1.5)) will be accurate except when the pulse duration is of the order of the reciprocal bandwidth.

In the following, we calculate as examples the Ψ function for some simple spectrogram shapes.

The Linear Chirp

The relation between ω and τ for a linear chirp is shown in Fig. 2.

$$\tau(\omega) = \tau(\omega_1) + a(\omega - \omega_1) \tag{1.7a}$$

$$\phi(\omega) = (\omega - \omega_1)\,\tau(\omega_1) + (a/2)(\omega - \omega_1)^2 \tag{1.7b}$$

Direct integration of Eq. (1.6) between the limits $-\infty$ and ∞ gives

$$\Psi(t) = (2\pi/a)^{1/2} e^{-i[\omega_1 \tau(\omega_1) - \pi/4]} \; e^{-i\left\{\omega_1[t - \tau(\omega_1)] + [t - \tau(\omega_1)]^2/2a\right\}} \qquad (1.8)$$

The carrier frequency at time t, given by differentiating the phase in Eq. (1.8) is $\omega_1 + [t - \tau(\omega_1)]/a$ corresponding to a frequency sweep rate a^{-1}. The amplitude of Ψ is constant.

The Double-Valued ω Case

The interesting cases are when $\omega(\tau)$ is a multiple-valued function of τ, which result in interference effects on the amplitude. In this section we consider two simple cases where ω is double-valued and $\tau(\omega)$ has one extremum. The results of the two cases, for which the spectrograms have the forms shown in Figs. 3 and 4, are qualitatively similar.

The parabolic characteristic is given by

$$\tau(\omega) = \tau_0 - \tau_1^3(\omega - \omega_0)^2 \qquad (1.9)$$

Using Eq. (1.6),

$$\Psi(t) = e^{-i\omega_0(t-\tau_0)} \int_{-\infty}^{\infty} e^{-i\tau_1^3\Omega^3/3} \; e^{-i\Omega(t-\tau_0)} \, d\Omega = (2\pi/\tau_1)\, e^{-i\omega_0(t-\tau_0)} \; Ai\left(\frac{t-\tau_0}{\tau_1}\right) \qquad (1.10)$$

Here Ai denotes the Airy function[12], which usually arises in turning-point problems[13]. The interference between the upper and lower branches of the parabola shows up as the successive pulsations of the square of the Airy function. If the parabola of Fig. 3 is rotated through 90°, τ becomes a double-valued function of ω and a sequence of maxima and minima described by the same Airy function appear in the pulse spectrum[14].

A similar case is illustrated in Fig. 4 where $\tau(\omega)$ varies sinusoidally across the bandwidth Ω and is at most double-valued.

$$\tau(\omega) = \tau_0 + \tau_2 \cos[2\pi(\omega - \omega_0)/\Omega] \qquad (1.11a)$$

$$\phi(\omega) = \omega\tau_0 + (\Omega\tau_2/2\pi) \sin[2\pi(\omega - \omega_0)/\Omega] \qquad (1.11b)$$

It is assumed that Ω spans the bandwidth of non-zero $|g(\omega)|^2$, so that in taking the Fourier transform in Eq. (1.6) we may integrate over the reduced range $-\pi$ to π for the veriable $2\pi(\omega - \omega_0)/\Omega$. Equation (1.6) becomes

$$\Psi(t) = (\Omega/2\pi) \; e^{-i\omega_0(t-\tau_0)} \int_{-\pi}^{\pi} e^{i(z \sin y - \nu y)} \, dy \qquad (1.12)$$

where $z = \Omega\tau_2/2\pi$ is one-half of the time bandwidth product, and $\nu = \Omega(t - \tau_0)/2\pi$. Equation (1.12) can be written

$$\Psi(t) = \Omega\, e^{-i\omega_0(t-\tau_0)} \quad \underset{\sim}{J}_\nu(z) \tag{1.13}$$

where $\underset{\sim}{J}_\nu(z)$ is the Anger function[15] defined by

$$\underset{\sim}{J}_\nu(z) = \frac{1}{\pi}\int_0^\pi \cos(\nu y - z \sin y)\, dy$$

Figure 5 depicts the square of the Anger function for a 100 cm^{-1} bandwidth and time-bandwidth products of 2, 6 and 20. Again the complexity of the pulse intensity resulting from a simple phase structure is illustrated. The TPF curve generated by the third Anger frunction of Fig. 5 is shown in Fig. 6 together with some TPF data reported by Shapiro and Duguay.[16] These authors have used other pulse models[17] to fit their data. Notice that the convolution of Eq. (1.5) was not made prior to the TPF computation. A taper in the spectrum would probably reduce the shoulders in Fig. 6 and thereby improve the fit. Many other spectrogram forms would fit the data equally well, because the TPF data contain so little information on the actual pulse structure.

Double-Valued ω With Two Turning Points

This case is modeled in Fig. 7, again with a sinusoidal variation as in Fig. 4. The phase is now

$$\phi(\omega) = \omega\tau_0 - (\Omega\tau_2/2\pi)\cos 2\pi(\omega - \omega_0)/\Omega \tag{1.14}$$

and with the same substitution as used in the previous section, the pulse is described by

$$\Psi(t) = \Omega\, e^{-i\omega_0(t-\tau_0)}\, \frac{2}{\pi}\int_0^\pi \cos\nu y\, e^{-iz\cos y}\, dy \tag{1.15}$$

This last integral can be expressed in terms of Lommel's functions.[15] Figure 8 depicts the intensity $|\Psi(t)|^2$ for the same bandwidth and time bandwidth products as were used in Fig. 5.

It should be clear from the above discussion that the dynamic spectrogram contains valuable information that is usually expressed otherwise in terms of pulse duration, bandwidth, amplitude modulation and phase modulation, and it is difficult to conceive of a measurement that conveys or obtains more information on a single pulse when the time reference is provided by the pulse itself. The next section of this paper is devoted to discussion of some experimental techniques for constructing the dynamic spectrogram.

Basic Principles of Measurement

Reference to Fig. 1 shows that the basic elements of the experimental apparatus should be a set (or continuum) of bandpass filters for the vertical axis and a clock for the horizontal axis. The realization of the filter system will be discussed first.

Consider the grating spectrometer[18] shown in Fig. 9. The principal quantities characterizing this instrument are its angular dispersion $d\theta/d\lambda$ (or $d\theta/d\omega$) and its resolving power $\lambda/\delta\lambda$. In terms of the grating constant d and order of diffraction m, the resolving power is given by

$$R.P. = m \frac{A_1 A_2}{d} \tag{1.16}$$

or m times the number of rulings intercepted by the beam. The number given by Eq. (1.16) is the smallest number of cycles that can be observed in a wave group at a point in the focal plant FF' for any short pulse input to the spectrometer. The angular dispersion is readily found from elementary grating theory, and it might amount to typically 10 to 20 Å per mm in the focal plane of a lens 50 cm focal length. A short pulse incident on the grating will become canted at an angle α after diffraction and at some instant will be clustered around the region (CC', DD'). It is readily shown that the canting is a fundamental consequence of the angular dispersion, in that

$$\cot\alpha = \omega \, d\theta/d\omega \tag{1.17}$$

for any dispersive element. Wavelength λ, clustered at some instant around CD passes through Λ in a minimum time of CE/c while λ' passes through Λ' in a time $(CE/c)(\lambda'/\lambda)$. The point Λ thus corresponds to a filter tuned to frequency $\omega = 2\pi c/\lambda$ with response time $\delta t = CE/c$ and bandwidth $\delta\omega = 2\pi/\delta t$. The filtering action at points P_1 and P_2 is different in that the response time still corresponds to the duration of R.P. cycles, but the bandwidth is now increased because all wavelengths in the range λ to λ' pass through P_1 and P_2 with λ preceeding λ' at P_1 and following at P_2. It is only in the focal plane that the bandwidth attains its $2\pi/\delta t$ value.

The wave groups CD and C'D' generated by a δ- function input pulse pass through Λ and Λ' simultaneously. A snapshot of the pulse (CC'; DD') at some later time would show the group (JJ'; KK') where obviously KK' precedes JJ'. Hence if one mistakenly believed that GG' was the focal plane it would appear that wavelength components around λ' always preceded those around λ in the original pulse. This is an important consideration in the fast spectrometer design discussed below.

The focal line FF' of the grating spectrometer thus provides the continuum of bandpass filters with enough angular dispersion, but the response time CE/c would be typically 100 to 200 psec for a small standard grating. The response time could be reduced by inserting another optical element that transforms the canted group (CC'; DD') into a group at right angles to the ray directions, like (DD'; EE'). However, if $\alpha = 90^{\circ}$, $d\theta/d\omega$ is zero and the angular dispersion is lost. One method of straightening out the canted group without changing α is to place a stepped mirror between the grating and lens as shown in Fig. 10. Since the reflection laws are obeyed at each step of the mirror, α is preserved but the beam P_1P_1' of Fig. 10 is chopped into many beams in the region P_2P_2', while the path lengths P_oP_2 and $P_o'P_2'$ are equal. One might say that the grating has been imaged by the stepped mirror into a stepped sequence of narrow gratings, where the considerations of Fig. 9 pertaining to response time δt apply to each narrow grating element, and where the stepped mirror block is swung to the appropriate angle to put all the δt's of the elements into the same time slot of duration δt.

Experimental Details

A spectrometer like that shown in the lower part of Fig. 10 has been built using sixty microscope slides of thickness 1.2 mm for the stepped mirror. The slides were stacked into a rectangular block and the end of the block was ground flat and polished. The block was then adjusted by placing the slide ends on a flat surface and tipping the stack through 18.5° and then clamping it. Under these conditions the response time δt is calculated to be 1.56 psec and the bandwidth at λ = 1.06 micron is 21.4 cm^{-1}. Mechanical imperfections raise these values somewhat, but the δt was verified to be about 2 psec[18], which is adequate for studying pulses of a few picoseconds duration.

It is clear that if the angular orientation of the fixed stepped mirror assembly is chosen to minimize the response time at wavelength λ, the response at λ' is not minimum, but for a range of approximately 100 Å or 200 Å around 10,600 Å there is not much spread in filter characteristics at the focal plane. Perhaps a better spectrometer design would eliminate this problem.

Another imperfection of the instrument is that the radiation reaching a given step of the mirror has arrived from a direction that is wavelength dependent because of the angular dispersion of the grating. The longer wavelength components reaching the step have come from points further downstream on the grating surface and this causes the pulse to be longer a P_2 than at P_2'. It also introduces into the spectrometer a group delay time as measured from P_oP_o' to the focal plane FF' of the lens that increases with wavelength. This effect is reduced by aperturing off part of the stepped mirror assembly and keeping the grating as close as possible to the stepped mirror.

When using the spectrometer an attempt is made to minimize the response time for the middle of the spectrum and a correction for the effect mentioned is calculated from the elementary diffraction grating theory by measuring the distance

along the mean ray direction from the center of the stepped mirror to the grating. In actual apparatus used the error amounts to 1.53 psec delay per 100 Å. This type of error can be avoided by designing the spectrometer such that the beam hits the stepped mirror before the grating.

The fast spectrometer just described is capable of producing time-resolved spectra with a 2 psec resolution time.[19] Subpicosecond response time could be achieved easily if the bandwidth warranted it, simply by using thinner plates in the stepped mirror.

When a pulse containing phase structure is passed into the spectrometer, wave groups of different frequencies pass through the focal line at different times determined by the time sequence of their occurrence in the pulse. If one could take a picture of the light in the focal region of the lens at an instant when the wave groups are passing through it, one would have the dynamic spectrogram of the pulse. This can be done in effect by photographing the fluorescence following two-photon absorption (TPF) when the light pulse intersects another short pulse in a cell of the dye Rhodamine 6G dissolved in ethylene dichloride[1]. In this technique the fluorescence is enhanced where the light pulses overlap and the motion of the second pulse provides the clock for the first as required for the horizontal axis of Fig. 1.

The actual experiment uses a variation of the above technique, wherein the pulse is made to intersect its inverted image in the focal plane. The upper portion of Fig. 10 shows the TPF apparatus used. The focal plane FF' lies in the center of the dye cell. The beam is passed through a beam splitter B.S. and the spectrum is displayed in both senses in the plane FF': the wavelength increases in the direction FF' in one beam and decreases in the other. Each point except one in the focal plane corresponds to two wavelengths. The wavelength at the unique point is called λ' in Fig. 11. Suppose that the pulse to be analyzed has a monotonically decreasing wavelength (a frequency up-sweep). As this pulse approaches the focal plane from two sides the wave groups will at some instant occupy the regions of space indicated by the outer sausage-shaped forms in Fig. 11. This figure also shows the enhanced fluorescence in the region of the focal plane, and it is this enhanced fluorescence that shows up on the photograph. Notice that the enhanced region is shown as an antisymmetric display as it always must be, for we are measuring not the true spectrogram itself, but another function corresponding to the antisymmetrization about λ'. The true spectrogram would give the time of arrival $\tau(\omega)$ of the wavegroups as a function of ω. In the present case, let the frequency corresponding to λ' be ω_o. Then the frequency $(\omega_o+\Delta\omega)$ intersects $(\omega_o-\Delta\omega)$ in the dye cell causing two photon absorption at $2\omega_o$, and the enhanced fluorescence region traces out the antisymmetric function $T_{\omega_o}(\Delta\omega) = \tau(\omega_o+\Delta\omega) - \tau(\omega_o-\Delta\omega) = -T_{\omega_o}(-\Delta\omega)$. In order to reconstruct $\tau(\omega)$ one would need to know the antisymmetrized functions above for several values of ω_o. Obviously the central slope of the middle sausage of Fig. 11 gives $d\tau/d\omega$ at $\omega = \omega_o$, which is the frequency sweep rate. (The 1.53 psec/100 Å correction discussed earlier has to be added on.)

The value of the self-intersecting ω_0 is easily adjusted and measured. A calibrated interference filter with a 10 Å wide passband is placed after the Galilean telescope of Fig. 10. The spectral plane FF' will then receive light at only two spots corresponding say to where the dashed lines intersect FF'. Knowing the wavelength dispersion in FF' and measuring the distance between the two spots (using for example burns on carbon paper placed in the plane FF') gives immediately the wavelength corresponding to the solid ray in FF'. If the lens in Fig. 10 is moved to the left the dashed rays move apart thus changing the self-intersecting wavelength. Hence ω_0 is readily adjusted in this instrument.

If the two mirrors M_1 and M_2 in Fig. 10 are replaced by a single mirror, the wavelength increases in the direction F'F in both beams, and one no longer has even the antisymmetrized spectrogram. However, this TPF displays the duration of the filter responses across the wavelength band, and this duration will equal the filter response time if the pulse has a sufficiently simple spectrogram. The stepped mirror may now be aligned to give the narrowest TPF, and this will correspond to the optimum spectrometer adjustment; i.e., minimum value of δt.

Some Experimental Results with a Mode-Locked Nd:Glass Laser

The usual method of examining picosecond pulses by TPF is to intersect the light beam with itself inside the dye cell.[1,4,17] Figure 1.12 compares the results of three types of TPF measurement. The top picture is the standard TPF from which one deduces pulse duration. The second picture is made in the way just discussed, and the fact that it is narrower than the top picture proves that the pulse has phase modulation. The bottom picture, shown for comparison, was made in the way indicated by Fig. 1.11, and it shows that the frequency sweep is positive. The slope of the central bright region proves that the pulses are phase modulated, with frequency increasing with time within each pulse. Were it not for the instrumentally introduced 1.53 psec/100 Å, the bright region would be tilted even further than shown. All three pictures were made using essentially the entire laser beam cross section and the entire pulse train. Measurements of phase structure on single pulses will be the subject of a future study.

A set of measurements[20] taking data like that in Fig. 1.11 is summarized in Fig. 1.13. The sweep rate is found by measuring the angle of tilt at the center of the display, and the results are shown in Fig. 13. The sweep rate at a given wavelength varies considerably from shot to shot, this variation being reflected in the spread indicated by the vertical bars in Fig. 13. (The particular laser on which the measurements were made does not exhibit a very reproducible pulse train on successive shots.)

It is instructive to attempt to interpret the results of pulse compressior experiments on the basis of the results shown in Fig. 13. One can draw a smooth line through the array of points to obtain a best fit in some sense. (For example, all the data can be fitted with a regression exceeding 0.75 by a curve of the form:

$$R = a_1 + a_2 \cos K(\lambda - a_3) + a_4 \cos 3K(\lambda - a_5)$$

for sweep rate versus wavelength, although there is no theoretical reason for choosing this particular form.) We consider a pulse having a frequency sweep rate given by the above relation as a typical pulse. Simple integration gives the curve labelled I in Fig. 1.14a for the relation between the group arrival time $\tau(\omega)$ and frequency ω. Curves II, III, and IV are derived from curve I by adding linear group delays of 3, 7, and 10 psec per 100 cm^{-1} and resetting the time origin in each case. These curves represent the frequency sweep characteristics that the pulse would have following pulse compression by a grating pair[7] with various settings of the spacing between the gratings. Obviously the pulse corresponding to the curve III has the smallest effective time-bandwidth product of the set, and is, therefore, compressed better than the others. Curves II and III each have two turning points, and are thus qualitatively similar to the case discussed in connection with Fig. 7.

Instead of computing $\Psi(t)$ as defined by Eq. (1.6) for the curves of Fig. 1.7 we assume a simple form for $g(\omega)$, which will be the same for each curve, and compute the pulse shapes. The form of $|g(\omega)|^2$ chosen is shown in the box in Fig. 1.14b. It consists of a pair of half Gaussian functions fitted together, the half widths being in the ratio of 2:1 and the total width between the $1/e^2$ points being 75 cm^{-1}. The spectrum peaks at the ω corresponding to $\lambda = 10580$ Å. The exact shape of the spectrum has not been measured, but the form of $g^2(\omega)$ chosen here is probably a fairly good approximation. Using the left side of Eq. (1.5) with g_v replaced by $|g|$ we obtain the pulse shapes (intensity versus time) shown in Fig. 1.14b. Pulse I is asymmetric with a longer rise time than fall time. This asymmetry is due to the unsymmetrical spectrum and was first detected in TPF experiments in which the pulse train was crossed by a train of compressed pulses.[6] The effect of the curvature at the ends of curve I in Fig. 1.14a is to make the initial rise and the fall at the end of the pulse more sudden than would arise from a purely linear frequency sweep. This same curvature causes turning points in curve II of Fig. 14a and thus leads to a double peaked pulse. Pulse III has a width at half intensity of 0.4 psec. Pulse IV is still of about one picosecond width at half intensity beacuse the energy in the wings of the spectrum is spread over a large time.

Conclusion

We have shown that the method of dynamic spectroscopy is adaptible to optical pulses in the picosecond regime. The present experimental work has involved the antisymmetrized spectrogram. The full spectrogram could be obtained in one shot by crossing the dispersed pulse with its compressed counterpart. So far, the method is capable of producing only half of the information available in the technique because we measure only time of response in any filter and not the phase

of response carrier. Application of the technique to the pulses from a mode-locked N -lass laser yields not only new information on the details of the phase structure in ypical pulse, but also gives results in accord with earlier measurements, such as pulse duration, pulse shape asymmetry, and pulse compressibility. The important application of this technique will be in the study of the phase structure of single pulses before and after their propagation through various optical media.

The author thanks several colleagues for valuable assistance during the course of this investigation. In particular, we acknowledge a stimulating discussion with Bruce Knight on the theoretical interpretation of spectrograms. Raymond Michaud made the stepped mirror, and R. Bodurtha provided valuable technical assistance in the experiments. Dr. R. Burdick computed the Anger and related functions as well as the TPF curve of Fig. 1.6. M. D. Sohn computed the pulse shapes in Fig. 1.14b.

SECTION II

Higher Conservation Laws for an Inhomogeneously Broadened Medium

The decomposition of intense pulses into a number of separate 2π pulses has been described by numerical methods for an inhomogeneously broadened medium.[21,22] It has been found that the final pulse amplitudes may be fairly accurately determined analytically by using higher conservation laws that are satisfied by the inhomogeneously broadened system. The conservation laws are a generalization of those for the completely unbroadened system that were reported previously.[23,24]

The conservation laws that are obtained by interchanging ξ and τ in Eqs. (2) and (3) of Ref. 23, Appendix A will express conservation laws obeyed by the electric field envelope since $\mathcal{E} = \sigma_\tau$. It has been found that the extension of these past results to include inhomogeneous broadening is readily accomplished. If the terms in the ξ derivative are retained while those in the τ derivative are suitably modified by employing the Bloch equations, one obtains the conservation laws

$$\frac{\partial \rho_n}{\partial t} + c\,\frac{\partial F_n}{\partial x} = 0 \tag{2.1}$$

where

$$\rho_n = F_n + T_n \tag{2.2}$$

and

$$F_2 = \frac{1}{2}\,\Omega^{-2}\tilde{\mathcal{E}}^2 \tag{2.3a}$$

$$F_4 = \Omega^{-4}\left(\frac{1}{4}\,\tilde{\mathcal{E}}^4 - \tilde{\mathcal{E}}_t^2\right) \tag{2.3b}$$

$$F_6 = \Omega^{-6}\left(\frac{1}{6}\,\tilde{\mathcal{E}}^6 - \frac{2}{3}\,\tilde{\mathcal{E}}^2\tilde{\mathcal{E}}_t^2 + \frac{8}{9}\,\tilde{\mathcal{E}}^3\tilde{\mathcal{E}}_{tt} + \frac{4}{3}\,\tilde{\mathcal{E}}_{tt}^2\right) \tag{2.3c}$$

$$T_2 = \Omega^2 \langle 1+N \rangle \tag{2.4a}$$

$$T_4 = \left[\tilde{\mathcal{E}}^2 \langle N \rangle + 2\tilde{\mathcal{E}} \langle \Delta\omega\, 2 \rangle - 2 \langle (\Delta\omega)^2\ (1+N) \rangle\right] \tag{2.4b}$$

$$T_6 = \Omega^{-2}\left[\frac{1}{9}\,\tilde{\mathcal{E}}^4 \langle N \rangle - \frac{4}{3}\,\tilde{\mathcal{E}}_t^2 \langle N \rangle + \frac{4}{9}\,\tilde{\mathcal{E}}^3 \langle \Delta\omega\, 2 \rangle + \frac{8}{3}\,\tilde{\mathcal{E}}_t \langle (\Delta\omega)^2 \rho \rangle \right. \tag{2.4c}$$
$$\left. - \frac{8}{3}\,\tilde{\mathcal{E}} \langle (\Delta\omega)^3\, 2 \rangle - \frac{4}{3}\,\tilde{\mathcal{E}}^2 \langle (\Delta\omega)^2 N \rangle + \frac{6}{3} \langle (\Delta\omega)^4 N \rangle\right]$$

in which $\tilde{\mathcal{E}} = \sqrt{\alpha' c}\,\sigma_T$ where, in notation used previously, $\alpha' = 2\pi n_o \omega_o \wp^2/\hbar c$ and the angular brackets $\langle\rangle_T$ indicate an average over the spectrum of inhomogeneous broadening.

Integration of Eq. (2.4) over the entire length of the host medium, assumed for convenience to be semi-infinite, and over all time leads to

$$\int_0^\infty dx\, \rho_n(x,t) = c\int_{-\infty}^{\infty} dt\, F_n(0,t) \tag{2.5}$$

The functions $F_n(o, t)$ may be calculated for a given pulse shape at $x = 0$ by using Eqs. (2.3a-b). After the pulse has propagated far enough into the material for the steady-state pulse shapes to evolve, one may write[21]

$$\tilde{\mathcal{E}}(x,t) = \sum_{i=1}^{N} (2/\tau_i)\,\mathrm{sech}\,(t - t_i - x/v_i)/\tau_i \tag{2.6}$$

where the τ_i are the pulse widths, the v_i are the corresponding pulse velocities and the t_i are merely time delays which separate the various pulses. The value of N is determined by the area under the pulse at $x = 0$. For $\pi < \theta_o < 3\pi$, $N = 1$, for $3\pi < \theta_o < 5\pi$, $N = 2$, etc. For each 2π pulse the response of the two-level systems in the vicinity of the pulse is given by[24]

$$\rho_i = -D_i \sin\phi_i \tag{2.7a}$$

$$N_i = -1 + 2D_i \sin^2(\phi_i/2) \tag{2.7b}$$

$$\mathcal{Z}_i = 2D_i \Delta\omega \tau_i \sin(\phi_i/2) \tag{2.7c}$$

where

$$\phi_i = \int_{-\infty}^{t} dt'\, \tilde{\mathcal{E}}_i \tag{2.8}$$

and

$$D_i = \left[1 + (\tau_i \Delta\omega)^2\right]^{-1} \tag{2.9}$$

There is, of course, a small region at the edge of the medium within which the pulse evolution into a sequence of 2π pulses takes place. In this region Eqs. (2.6) and (2.7) are inapplicable. An unknown amount of the population is left in an inverted state and values of the polarization $\mathcal{P}$ and $\mathcal{Q}$ are similarly unknown. In performing the spatial integration in Eq. (2.5), this fact is neglected and Eqs. (2.6) and (2.7) are used over the entire range of the spatial integration. The closeness of the results thus obtained to those predicted by the exact numerical calculation shows that, as for the Korteweg-deVries equation[25,26] this transient region may indeed be ignored. For weaker initial pulses which result in only a single 2π pulse, however, this initial region is no longer negligible. Hence only pulses which have an initial area greater than 3π are considered in the following.

For the initial pulse profile

$$\tilde{\mathcal{E}}(0,t) = (\theta_0/\pi t_0)\,\mathrm{sech}\,(t/t_0) \tag{2.10}$$

one finds

$$t_0\int_{-\infty}^{\infty} dt\, F_2(0,t) = (\theta_0/\pi)^2 \tag{2.11a}$$

$$t_0\int_{-\infty}^{\infty} dt\, F_4(0,t) = \frac{2}{3}(\theta_0/\pi)^2\left[\frac{1}{2}(\theta_0/\pi)^2 - 1\right] \tag{2.11b}$$

$$t_0\int_{-\infty}^{\infty} dt\, F_6(0,t) = (56/45)(\theta_0/\pi)^2\left[\frac{1}{7}(\theta_0/\pi)^4 - \frac{5}{7}(\theta_0/\pi)^2 + 1\right] \tag{2.11c}$$

Also, substitution of Eqs. (2.6) and (2.7) into Eq. (2.2) and integration over the entire length of the medium yields

$$\int_0^{\infty} dx\,\rho_2 = 2c\sum a_i \tag{2.12a}$$

$$\int_0^{\infty} dx\,\rho_4 = \frac{1}{3}c\sum a_i^3 \tag{2.12b}$$

$$\int_0^{\infty} dx\,\rho_6 = \frac{1}{5}c\sum a_i^5 \tag{2.12c}$$

where $a_i = 2/\tau_i = (\mathcal{E}_i)_{max}$. As noted above, one expects two pulses for $3\pi < \theta_o < 5\pi$. In this case only the first two conservation laws are needed and one finds

$$\begin{aligned} a_1 + a_2 &= \tfrac{1}{2}\int dt F_2 \\ a_1^3 + a_2^3 &= 3\int dt F_4 \end{aligned} \tag{2.13}$$

For $5\pi < \theta_o < 7\pi$, three pulses will be obtained. Hence one requires the solution of

$$\begin{aligned} a_1 + a_2 + a_3 &= \tfrac{1}{2}\int dt F_2 \\ a_1^3 + a_2^3 + a_3^3 &= 3\int dt F_4 \\ a_1^5 + a_2^5 + a_3^5 &= 15\int dt F_6 \end{aligned} \tag{2.14}$$

One sees from Eqs. (2.3a-b) that the higher conservation laws depend upon higher derivatives of the initial pulse shape. Hence the decomposition of strong pulses is expected to be sensitive to the detailed structure of the initial pulse profile. Such sensitivity has been noted in experimental observations.[27]

In Fig. 15 the roots of Eqs. (2.13) and (2.14) divided by $\mathcal{E}(o, t)_{max}$ are plotted as a function of θ_o. Equation (2.13) possesses solutions for values of θ_o for which three pulses are to be expected. The locus of these unphysical solutions is given by the dashed portion of Fig. 15. The crosses are results obtained from numerical solutions of the equations which describe optical pulse propagation and are seen to be in quite good agreement with the approximate values obtained from the conservation laws. The numerical results include cases in which t_o/T_2^* varies from 0.1 to 10. The lack of complete correspondence is due partly to the improper treatment of the initial region in which the isolated pulses have not formed and partly to the fact that the correct amplitudes must satisfy all the higher conservation laws and not merely the lowest two or three that have been used here. Further work on this subject is currently being pursued.

SECTION III

Transient Stimulated Raman Scattering

In the previous annual technical report (J920479-21) extensive experimental data were presented on transient stimulated Raman scattering in liquids and gases. With the exception of the time delay between the generated Stokes pulse and the incident laser pulse, the experimental work succeeded in verifying all of the theoretical predictions concerning transient stimulated Raman scattering. In a recent reexamination of transient Raman scattering with picosecond pulses, carried out in collaboration with R. L. Carman at Harvard University, we have succeeded in a more quantitative comparison of theory and experiment and have observed for the first time the predicted Stokes pulse delay.

The following discussion is based on a paper entitled "Experimental Investigation of Transient Stimulated Raman Scattering in a Linearly Dispersionless Medium" by R. L. Carman and M. E. Mack that has been prepared for submission to the Physical Review.

Stimulated Raman scattering (SRS) induced by picosecond duration light pulses has been discussed by many authors from both an experimental[28] and theoretical[29,30] point of view. Realistic numerical calculations in this transient regime recently performed took into account practical laser pulse shapes in predicting the Stokes pulse duration, the SRS gain, and the delay between the peak amplitudes of the Stokes and laser light pulses.[30] Earlier experimental work suggested that in the case of picosecond duration light pulses generated by a mode-locked ruby laser, the Stokes pulses were certainly no longer in duration than the pump pulses.[31] Three serious limitations to this earlier work were the presence of strong self focusing in the CCl_4. the lack of control in the gain leading to a high probability of saturation and laser depletion, and the presence of significant linear dispersion, the deleterious effects of which were indicated in previous work. Here we present data on a system with negligible dispersion which verifies many features of the numerical results under conditions where self focusing and laser depletion can be neglected. In addition, the data add further support to the notion that the pulse should have a time dependence which is close to Gaussian.[32]

Of vital importance to a careful study of transient SRS is the absence of the effects of both linear dispersion and self focusing. As a result, much effort was expended in selecting a material which would minimize both. Linear dispersion tends to cause the Stokes wave packet to either speed ahead (normal dispersion) or lag behind (anomalous dispersion) the laser wave packet. Since the transiency introduces a delay of the Stokes amplitude peak with respect to the laser amplitude peak, dispersion will either improve or degrade the synchronism of the two wave packets, or more importantly of their phases. The net result is an alteration of the parameters associated with the Stokes pulse, including the magnitude and

dependence of the gain coefficient. The criteria for determining the importance of dispersion was presented in earlier work.[30] For dispersive effects to be negligible, the phase synchronism length determined by dispersion must be much greater than the length required for the gain to restore the constant phase difference between the laser and Stokes field. This is the case if

$$\frac{\pi}{\left|\left(\frac{\partial k}{\partial \omega}\right)_L - \left(\frac{\partial k}{\partial \omega}\right)_s\right| c\Delta\bar{\nu}} >> \frac{2\Delta\bar{\nu}}{g_{ss}\Gamma}, \tag{3.1}$$

where $\Delta\bar{\nu}$ is the laser pump line width in the medium, $e^{g_{ss}z}$ is the steady state SRS gain for the same intensity, and Γ is the molecular vibrational line width all expressed in units of cm^{-1}. Thus, the quantity to be minimized is

$$(\Delta\bar{\nu})^2 \; c\left|\left(\frac{\partial k}{\partial \omega}\right)_L - \left(\frac{\partial k}{\partial \omega}\right)_s\right|$$

It is clear from Eq. (3.1) that it is unwise to use a laser whose bandwidth is much larger than is required to cause a transient response if dispersive effects are to be made small. At this point, it is convenient to define the ratio of the velocity of light in vacuum and the group velocity of the wave packet in the medium, n_g, which is basically the analog of the index of refraction, n, in the case of the phase velocity, or

$$n_g \equiv c\frac{\partial k}{\partial \omega} = n - \lambda\frac{\partial n}{\partial \lambda} \tag{3.2}$$

where λ is the wavelength of the light in vacuum. Restating Eq. (3.1), in terms of the group index difference $\Delta n_g = \left|(n_g)_L - (n_g)_s\right|$, we find

$$\Delta n_g << \frac{\pi g_{ss}\Gamma}{2(\Delta k)^2} \tag{3.3}$$

In Table I, both n and n_g are given for the number of gases at atmospheric pressure and 0°C. For purposes of comparison, a few liquids are also included. The values of Δn_g indicated for the gases are those obtained by scaling up linearly to the typical operating pressure at which vibrational SRS would be observed. When the operating pressure is close to the liquification pressure at room temperature, one should scale with the density as was done for SF_6 in Table I instead of with pressure. In the other materials operated close to liquification, Δn_g in the table is too low by the ratio $\rho_{op}/(\rho_{1\,atm}P)$. Even at the very high required pressure gases are more than an order of magnitude less dispersive than are liquids.

The gases listed in Table I represent relatively high Raman gain materials which are available at reasonably high pressure and whose stimulated Raman shifted components have been observed.[33] In addition to the vibrational SRS component, the rotational analog has also been observed with picosecond pulse excitation[33] for the cases of N_2O, CO_2, and O_2. In Table II, estimates of the transient vibrational SRS gain and the rotational Raman γ^2 are given, where γ is the anisotropic part of the molecular polarizability tensor. The rotational SRS cross section is proportional to γ^2. It is clear from Table II that both ethylene and chlorine gas should also have stimulated rotational Raman bands. The existence of rotational SRS is important because it represents a competing mode of operation and because it effectively increases the line width $\Delta\bar{\nu}$ of the pump causing dispersion to be more important for the vibrational SRS. Therefore, all five gases, N_2O, CO_2, O_2, Cl_2 and C_2H_4 must be eliminated as sample candidates.

Of the remaining ten gases in Table I, SF_6 is the least dispersive by a factor between two and fourty-five. Although values of $\partial\alpha/\partial R$ and R are not available for SF_6, the very low threshold for transient vibrational SRS as well as the very high conversion efficiencies (up to 70%) observed experimentally[33] indicate a large vibrational Raman cross section. In addition, we have never observed rotational SRS in SF_6 under any conditions.

The remaining question of the importance of self-focusing effects at our required operating conditions was then investigated for SF_6. A mode-locked ruby laser was used which produced approximately 10 to 15 millijoules per pulse within a 0.5 x 1.0 cm elliptical cross section at a divergence angle of between 0.5 and 1 milliradian.[34] The output intensity profile was locally uniform over at least 2 mm. Near field photographs of the collimated beam passing through a 50 cm cell were indistinguishable with and without gas. Also, investigations were made of both the laser and Stokes beam spatial profile in the case of focusing the pump with a 50 cm lens.[35] Again no spatial effects were attributable to self focusing. Finally, using the measured self-focusing threshold in liquid SF_6,[36] and extrapolating to gas density indicates that much higher field strengths would be required for self focusing to be important than are needed for SRS.

The experiments were performed with the mode-locked ruby laser described above at output energies of between 5 and 10 millijoules per pulse. The beam was focused with a one-meter focal length lens into the 50 cm long cell of SF_6. The SF_6 operating pressure was 18 atmospheres. The diagnostics are illustrated in Fig. 17. Both incident and transmitted laser energies per pulse were monitored by photodiode #1, and data was taken only when both signals were the same height to within 5% for each pulse. At such a low conversion efficiency, overall laser depletion is not important. In the absence of self-focusing local laser depletion effects are avoided as well. A second fast rise time photodiode (#2) monitored the Stokes energy generated per pulse. Figure 17 shows corresponding laser and Stokes pulse trains under strong conversion conditions. Typical laser depletion oscillograms are shown in Figs. 18a and 18b under acceptable conditions. Figure 18a shows the result of either raising the laser output or changing to a 50 cm focal length lens at the cell input.

The two photon absorption fluorescence setup, illustrated in Fig. 16, was isolated from the experiment by Filter #3, which had a factor of 100 attenuation per pass at the laser frequency. Filter #3 also had the property of making the laser and Stokes intensities comparable under the operating conditions described above. A cylindrical lens was used to intensify the overlap region and had the additional advantage of reducing the depth of field requirements of the camera lens. Filters #5 and #6 were of equal optical path length, and were used in the following three modes in conjunction with Filter #4: (1) Filters #5 and #6 were removed completely and Filter #4 was an IR cutoff filter transmitting just the laser beam. This resulted in a laser pulse duration measurement. (2) Filters #5 and #6 were removed completely and Filter #4 was a UV cutoff filter transmitting just the Stokes beam. This resulted in a Stokes pulse duration measurement. (3) Filter #4 was absent, and Filter #5 was a UV cutoff filter while Filter #6 was an IR cutoff filter. This resulted in running the forward directed laser beam against the beamsplit Stokes beam. This display should have been undisplaced from that of conditions (1) and (2) if no delay existed and the pulse duration measured in (3) should be that of the longer pulse duration. For good contrast in the two photon absorption-fluorescence photographs, the Stokes and laser intensities in the overlap region must be nearly equal. Because we require operation, which avoids saturation and laser depletion, small fluctuations in the laser output intensity results in large variations in the relative Raman cell output beam intensities. As a result a large number of laser firings were required to obtain useable data.

In order to avoid errors due to a systematic change in the operation of the laser, data was taken in cycles, where each cycle involved going through the above modes sequentially. Using about 2.5 psec duration laser pulses, the Stokes duration t_s was consistently, about a third shorter than the laser duration t_L. This is in contrast to the CCl_4 work[31] where $t_s > t_L$ as well as $t_s < t_L$ was encountered. A typical output display for the 2.5 psec duration excitation is shown in Fig. 19.

Using these short pulses, it would be very difficult to determine quantitatively the size of any delay between the laser and Stokes pulse peaks since the delay would be expected to be less than one laser pulse duration.[30] Consequently, the laser pulse duration was lengthened to $\tau_L \approx 15$ psec. The time-bandwidth product remained at unity.[34]

In Fig. 20 we show two traces of the spontaneous Raman line width, Γ, of the 775 cm^{-1} mode in SF_6, which indicate that the response will still be transient with the longer pulses. Trace (a) was taken using a Spex double grating monochromator in conjunction with an argon laser operating on the 5145 Å line. The measured width was 2.75 cm^{-1} for the Stokes plus slit function, while the laser line measured 1.1 cm^{-1} (pure slit function), corresponding to an actual line width for the SF_6 775 cm^{-1} mode or $\Gamma \cong 1.65$ cm^{-1}. Trace (b) was taken using a piezoelectrically scanned Fabry-Perot interferometer in conjunction with a multichannel analyzer and the same argon laser. While 90-minute integration times were required with a one second scan time, the very weak signal was sufficiently

large after filtering out the laser line to yield a line width of 1.4 ± 0.2 cm^{-1}. The two methods were in good agreement, and a pulse duration of 15 psec was, therefore, justifiable since the condition for transiency is that $\Gamma \ll G_{ss}\Delta\nu$ where $e^{G_{ss}}$ is the steady state gain assuming the same incident intensity. Since oscillation requires $G_{ss} > 10$, this relationship is satisfied.

The results of experiments carried out with the 15 psec duration excitation are shown in Fig. 21. The relevant quantities are for a laser pulse duration $t_L = 15$ psec, the Stokes pulse duration $t_s = 9$ psec, and the delay between intensity maxima $t_o = 6$ psec. This represents the first experimental verification of the delay as well as the first clear demonstration of the pulse shortening.

In Fig. 22, we have reproduced for the sake of completeness some of the numerical results[30] which are relevant to these experiments. An important parameter is the product of Γ and $t_L = 1/\Delta\nu$, and for the 15 psec duration laser pulses, $\Gamma t_L \approx 1$. The second important piece of information is the laser pulse shape. Figure 22 is for a Gaussian temporal distribution for the laser, and it shows that for $t_s/t_L = 0.6$ we have a transient gain e^{G_t} where $G_t \approx 9$. Reading vertically, we then find that $t_D/t_L = 0.42$ which is in reasonably good agreement with the experimental value. Finally, the corresponding steady state gain would be $e^{G_{ss}}$, where $G_{ss} = 25$.

Since all the two photon absorption fluorescence data were not taken simultaneously, one cannot choose with certainty between various models for the ruby laser pulse shape. However, if the time variation of the laser electric field envelope is assumed to be of the form $E_L \propto e^{-|t/T|^n}$, the multiple shot data described above indicates that n must be in the range $1.5 < n < 3$, where $n = 2$ is the Gaussian.

These experiments confirm enough of the details of the transient SRS theory to provide a reasonable confidence in its validity. However, a lack of linear dispersion is the exception in the historically important Raman active materials, as well as in long range atmospheric pressure gas paths. Due to the difficulty of the numerical calculations which include linear dispersive effects, experimental confirmation of the present theory under exceptionally clean and simple conditions is very important. These experiments provide that confirmation. In addition, calculations on self-induced transparency and other coherent effects associated with the stimulated Raman process require a complete understanding and description of the low field effects. Finally, an understanding of the competition between various nonlinear processes such as rotational SRS with vibrational SRS, frequency broadening with SRS, self focusing with various inelastic stimulated scattering processes, etc., depends on how well we can model the independent processes.

From an experimental point of view, the feasibility of determining approximate laser pulse shapes using SRS has been demonstrated for the simple case of a time-bandwidth product one pulse. In the more complicated cases of the mode-locked Nd:glass laser or mode-locked organic dye lasers, one may hope to learn something about the reproducibility of any temporal structure, as well as the effective rate

of rise and fall of the envelope of any temporal structure. However, the wider laser pulse bandwidth and large time bandwidth product $t_I\Delta\nu$ implies that dispersive effects will play a more important role. In order to do a similar experiment to the one reported here, higher intensities and shorter cell lengths would have to be employed. The condition on the intensity can be obtained directly from Eq. (3.3), namely,

$$g_{ss} >> \frac{2(\Delta\bar{\nu})^2\Delta n_g}{\pi\Gamma}. \tag{3.3}$$

Therefore, for the same magnitude of Δn_g and degree of satisfaction of the inequality the laser intensity must scale quadratically with the bandwidth. This implies that for the same transient gain that the interaction length z would scale inversely with approximately the laser bandwidth squared times the laser pulse duration.

Vibrational Decay Measurements in Gases

Several experiments are presently in progress to exploit transient stimulated Raman scattering for vibrational decay measurements in gases. Other techniques for vibrational decay measurement as for example shock tube analysis, require elevated temperatures to produce the necessary vibrational excitation. Stimulated Raman scattering provides a unique method for producing a relatively large non-equilibrium vibrational population at room temperature or below if desired. For gases other than hydrogen or methane picosecond pulse excitation must be used in order to avoid detrimental Brillouin competition.

Having produced the necessary vibrational population several techniques are available to monitor its decay. For gases having an allowed infrared transition from the excited (v = 1) vibrational state, normal fluorescence may be used to determine the decay rate. Such experiments are now in progress in carbon monoxide. An infrared signal at the proper wavelength has been detected but it has not yet been determined whether this represents actual fluorescence or a non-linear parametric down conversion (the 2000 cm^{-1} line in CO is both infrared and Raman active). For gases lacking an infrared active transition from the vibrationally excited state, there are two other techniques for monitoring vibrational decay. The first involves detecting in a Schlieren system the index of refraction changes which result from the thermalization of the vibrational population. Although simple in principle, this technique is subject to other laboratory perturbations and so can be difficult to implement in practice. The second technique involves the use of a second laser, producing spontaneous anti-Stokes scattering from the excited vibrational population. This latter technique is highly specific but the signal levels can be quite low. Both techniques are being tested. Progress will be reported at a later date.

SECTION IV

Dye Lasers

Ultrafast Capillary Flashlamps

In the previous technical report, J920479-23, the basic circuit design for the ultrafast capillary flashlamp was described and preliminary operating data was presented. A 2.8 joule, 38 kV version of this device has been built and tested for dye laser pumping. As in the previously described units the energy is carried in two, 1.2 mm bore, 3 mm O.D. capillary flashlamps with an arc length of 26 mm. One valuable feature of these lamps not noted previously is that at the present energy loading the lamps are self-cleaning. Evaporated quartz and tungsten electrod material is blown out of the arc region past the electrodes by the force of the discharge. The same situation has been found to occur in slower rise time capillary lamps of similar construction.[37]

In the present capillary flashlamp unit lead inductance has been reduced to a minimum. The 10 - 90% flash rise time is approximately 12 nanoseconds and the flash duration (FWHM) is about 50 nanoseconds. As in the previous devices the effective color temperature is very high, on the order of 100,000°K, and as a result, the optical energy conversion efficiency is somewhat low, about 2% in the range from 2200 Å - 5000 Å.

Using a polished aluminum foil reflector, the two capillary flashlamps are close coupled to a 4 mm O.D., 3 mm I.D., 35 mm long quartz dye cell. Lasing was easily achieved with a number of the xanthene dyes including sodium fluorescein, rhodamine 6G, and rhodamine B. With a mirror reflectivity product of 0.9, lasing could be produced in ethanol solutions over a broad range of concentrations, from 10^{-4} M to room temperature saturated solutions ($>10^{-2}$ M). Optimum output occurred with a concentration of about 10^{-3} M and a mirror reflectivity product of 0.5. With this arrangement the peak power output was from 1 - 5 kilowatts and the energy output was ~0.1 - 0.5 millijoule. At high concentrations (near saturated solutions) sodium fluorescein and rhodamine 6G produced a superfluorescent emission in a ring shaped near field pattern.

Despite the strong gain observed in the above dyes, few of the other normally strongly lasing dyes could be made to lase with the fast rise time flashlamp. Of the blue emitting dyes only the coumarin, 7-diethylamino-4-methyl coumarin, could be lased and then only over a very narrow range of concentrations with a mirror reflectivity product >0.95. None of the scintillator dyes could be made to lase despite the better match between their primary absorption bands and the strongly peaked UV emission of the flashlamps. This rich UV emission may be the source of the difficulty. The intense ultraviolet radiation may populate excited states in the dyes which are absorbing at the lasing wavelength. Such a situation does occur in other lasers such as, for example, the Nd:YAG laser. This possibility

will be investigated further upon completion of the 10 joule fast rise time flashlamp described later on in this section.

Several interesting transient effects are observed with the fast flashlamp pumped xanthene dye lasers. Figure 23 shows the results obtained using a 2×10^{-3} M ethanol solution of sodium fluorescein. The cavity mirror reflectivity product was 0.9. For the four photographs shown in Fig. 23, the oscilloscope was triggered using the output from a second photodiode which was set up to observe the flashlamp. Successive photographs of the flashlamp output (Fig. 23a) indicate that the jitter in the oscilloscope triggering is negligible on the time scale of Fig. 23. The laser output (Figs. 23b - 23d) is seen to be delayed and in Figs. 23b and 23c, at least, is seen to begin with a prominent initial spike. This initial spiking has also been observed in the case of laser pumping.[38] It must be noted that the delay exhibited in Figs. 23b - 23d truly represents a delay and not simply the time needed for the pump light to reach the required pumping threshold. In Fig. 23b, for example, the lasing begins near the peak of the pumping pulse (Fig. 23a) yet it continues until the pumping pulse is nearly over.

The origin of the initial spike and the cause for the delay are easily understood. At the beginning of the pumping pulse the photon density in the gain bandwidth of the dye is very low. As time goes on the inversion will build up due to the continued pumping and the photon density will grow due to fluorescence. The inversion will increase until the fluorescence is amplified to such a level that the loss of inversion through stimulated emission balances the increase due to the pumping. If the pumping rate increases sufficiently rapidly this maximum inversion can be several times the normal threshold inversion. The laser then emits a giant pulse in much the same way a Q-switched laser does. The so called "hair trigger mode"[39] of ruby laser operation closely parallels the present situation. The delay time observed in Figs. 23b - 23d is just the time required for the photon density to be amplified to a level sufficient to deplete the inversion by stimulated emission. A similar delay also occurs in Q-switching. These effects of transient pumping observed here in the ultrafast flashlamp pumped dye laser have also been noted in the atmospheric pressure CO_2 laser[41] and in the iodine flash photolysis laser.[42]

The natural time scale for transient pumping effects as for Q-switching (see ref 40) is the cavity decay time, which is the cavity round trip transit time divided by the fractional photon loss per round trip. For equal initial inversions (as measured in terms of the threshold inversion), the initial spike rise time and the delay time will scale with the cavity decay time. Sorokin[38] has already noted that the spike rise time decreases with increased output coupling. In Fig. 23 the cavity decay time has been varied by changing the cavity length. To the extent that diffraction losses are negligible this leaves the initial inversion unaffected. Figure 23 shows very clearly the increase in rise time and delay time with increased cavity decay time. The increase is slightly more rapid than a linear proportionality due to the loss of inversion by spontaneous decay during the delay period. This also accounts for the decreased peak power in going from the 9 cm cavity to the 25 cm cavity.

Fast Rise Time Unconfined Discharge Lamps

The capillary flashlamps discussed in the previous section suffer from several important drawbacks. The one millimeter bore, 3 millimeter O.D. capillaries will safely handle about 0.5 joule per centimeter of arc length. A 10 joule lamp, then, would have to be 20 cm long. An immense voltage would be required to break down such a lamp unless the gas pressures were lowered below atmospheric. However, reducing the pressure has been found to reduce the light output. In addition, the inductance of such a long narrow arc would be rather high. Some improvement in energy handling capability can be gained by increasing the capillary bore diameter or by increasing its wall thickness. Unfortunately, if the bore diameter is increased much beyond one millimeter the discharge is found to meander around the walls down the lamp. The light output is decreased and the rise time is increased. Increasing the wall thickness of the capillary does give some gain in energy handling capability. However, an order of magnitude improvement in energy handling would require an inordinately thick lamp.

These difficulties are overcome in the unconfined discharge lamp. This type of lamp consists very simply of a pressurized spark gap with transparent (fused quartz) walls. The discharge is unconfined in that the arc size (and position) are not determined by the walls of the lamp. This fact has several rather important consequences. There is substantially more volume available for shock wave dissipation in this type of lamp than in the more usual type of lamp. Consequently, the lamp has a relatively high energy handling capability. Since the envelope walls are removed from the arc and since the gas pressure is high (>1 atmosphere), wall deposits are greatly reduced, thus, increasing the useful lamp lifetime substantially. The open construction of the lamp permits the use of massive, cool running electrodes. Despite the simple, open construction, low inductance structures (to 2×10^{-8} H) are easily made.

Initial testing of the fast rise time unconfined discharge lamp was carried out using a lamp consisting of a 2.9 cm O.D., 2.5 cm I.D. by 10.0 cm long piece of fused quartz with $\frac{1}{4}$ in. diameter tungsten electrodes inserted through aluminum plates fastened to the tube ends. The electrode spacing was adjustable. Various size ringing inductors were used in the discharge circuit (see technical report J920479-23) giving breakdown delay times of from 100 nsec to 400 nsec. The results for a 200 nsec breakdown delay time are representative and are included here. The stored energy at the 35 kV operating voltage was 2.5 joules (4000 pf total capacitance).

With the present circuit arrangement, if the fill gas or the gap separation is changed, the gas pressure must be adjusted to give the required breakdown delay time, in this case 200 nsec. Figure 24 shows the gas pressure needed for a 200 nsec delay as a function of gap separation for four of the fill gases tried, air, nitrogen, carbon dioxide, and argon. The pressure required is seen to increase rapidly as the gap separation is reduced.

Figure 25 shows the temporal distribution of the output flash. The 10 - 90% flash rise time was 10 nsec independent of the fill gas and arc length except for the very short arcs where appreciable circuit ringing was encountered. The peak power of the lamp and the flash duration depended strongly on the gap separation and the f ll gas used as indicated in Figs. 26 and 27. The peak power outputs are remarkably similar for the different gases. The flash output durations on the other hand vary considerably from gas to gas. With a 1.2 cm gap separation the output duration varies from 35 nsec with nitrogen or air to 140 nsec with xenon as the filling gas. Since the peak light outputs are about the same, this indicates that the total energy output with the xenon is about four times higher than with nitrogen or air. The electrical to optical conversion efficiency in the range from 2200 - 5400 Å for the xenon was about four percent. The decrease in peak light output and the increase in flash duration is very likely due to the inability of the driving circuit to match the low impedence of the short arc. With gap spacings in the 0.2 - 0.5 cm range substantial ringing was observed in the flash output.

Tests similar to those described above have been run at the 5.0 joule input level (35 kV, 8000 pf total capacitance) using a one centimeter arc length and nitrogen and xenon as the fill gases. With either gas the 10 - 90% rise time was again 10 nsec. Curiously with the higher energy input the peak power outputs and the flash durations with the two gases were nearly the same. The optical conversion efficiencies were between two and four percent for both gases.

Preliminary life testing was carried out at the five joule input level. The gap separation was 1.0 cm and air was used as the filling gas. No particular care was taken in cleaning the lamp electrodes and the lamp jacket, nor was the air used for filling the lamp in any way cleaned or purified. The lamp was fired at from three to five pulses per second. the lamp lifetime to half power output was found to be in excess of 40,000 shots. It is quite likely that this can be extended substantially by better preassembly cleaning procedures and possibly by flowing the gas through the discharge region.

Under construction now is the integrated flashlamp-capacitor unit shown in Fig. 28. This unit consists of two mylar insulated 4000 pf, 50 kV, parallel plate capacitors with an arc lamp built into the center. The unit would store 10 joules of energy at its maximum charge voltage. The parallel plate storage capacitors offer a much lower inductance than the barium titanate capacitors used in the tests described above. The major inductance in the circuit is that of the lamp, about 20 nH.

The small arc volume and the open construction of the unconfined discharge lamps necessitate the use of some type of imaging to couple the flashlamp output into the dye cell. The coupling cavity should be axially symmetric about the arc for greatest arc stability. A spherical pumping cavity of the type shown in Fig. 29 has been constructed. The arc lamp is located along the axis of the sphere near the bottom. Spherical abberation results in an extended image along the upper axis of the sphere. Computer simulation has shown that the on axis

intensity is uniform to ± 50% over the central 1.5 in. of the image. Other types of imaging cavities, such as an elliptical cavity or a double parabola, were investigated but these were dropped from consideration because of their higher fabrication costs and because they offered only a slight improvement at best.

The spherical cavity which has been made consists of two 8 in.dia. mating, spun hemispheres, whi h have been polished on the inside and coated with evaporated aluminum. The dye cell is 2 in. long and protrudes through the top of the upper hemisphere. Four 1/8 in.dia. stainless steel tubes carry the liquid through the cavity to the bottom of the dye cell. These very little of the pump light. The dye laser cavity consists of a fused silic roof prism mounted within the sphere and dielectric mirror mounted directly on top of the sphere. The overall length of the optical cavity is only 8 cm.

High Power Flashlamps

The open discharge lamp discussed in the previous section for fast rise time applications is also well suited for slower rise time, high efficiency, high power operation. When operated in a simple static breakdown circuit the rise time of the output flash degrades but the optical efficiency improves. With 200 - 300 nsec rise time operation up to 20% electrical to optical conversion efficiency has been observed. The lamp is ideal for high repetition rate operation. As noted earlier wall deposits are minimized and heavy electrodes may be used. As a result of the high pressure the deionization is rapid. If very high repetition rates are desired a fast flow of fill gas through the discharge region can be used both to replenish the gas in the lamp between shots and to some degree to cool the lamp.

Two high power flashlamp units have been built and tested. The first used a low inductance, 0.6 μf Maxwell Laboratories capacitor operated at 6 kV (~ 10 joules). This lamp had a gap separation of one centimeter and used argon as the fill gas. The argon was flowed through the lamp at a rate of 10 - 30 liters (STP) per minute and at a pressure of about 1 atm. The flash rise time was 250 nsec and the flash duration (FWHM), 1.2 - 1.5 μsec. The electrical to optical conversion efficiency was in the range of 7 - 14%.

This lamp has been operated at repetition rates of up to 120 pps giving the lamp an average power dissipation of approximately 1.2 kilowatts. The life to half power output for this lamp was in the range of 10,000 to 50,000 shots, limited primarily by evaporation of electrode material onto the quartz envelope. For the sake of expediency the electrodes had been made of steel.

The second high power discharge lamp utilized a 25 kV, 0.3 μf (100 joule) low inductance, high repetition rate coaxial capacitor. The lamp was designed to be used with the same spherical pumping cavity as the fast rise time discharge lamp described in the previous section. The gap separation in this lamp is 2 cm. The fill gas is an argon-nitrogen mixture which is flowed through the lamp at 2 - 3 atm. and at a flow rate of 1 liter per second. The lamp has been tested at

energy inputs of up to 75 joules per pulse and at average power inputs of several hundred watts (presently limited by the power supply). At 50 joules per pulse the rise time is 200 nsec, the duration (FWHM) is 1.1 μsec and the electrical to optical conversion efficiency is 9 - 18%. In contrast to the previous lamp this device uses tungsten electrodes. This lamp should be an ideal pump source for a high output dye laser. It will be tested for this purpose shortly.

REFERENCES

1. DeMaria, A. J., W. H. Glenn, M. J. Brienza and M. E. Mack: Picosecond Laser Pulses. Proc. IEEE 57, 2-25 January 1969.

2. DeMaria, A. J., D. A. Stetser and W. H. Glenn: Ultrashort Light Pulses. Science 156, 1557-1568, June 1967.

3. Armstrong, J. A.: Measurement of Picosecond Laser Pulse Widths. Appl. Phys. Letters, 10, 16-17, January 1967.

4. Giordmaine, J. A., P. M. Rentzepis, S. L. Shapiro and K. W. Wecht: Two-Photon Excitation of Fluorescence by Picosecond Light Pulses. Appl. Phys. Letters 11, 216-218, October 1967.

5. Treacy, E. B.: Compression of Picosecond Light Pulses. Phys. Letters 28A, 34-35, October 1968.

6. Treacy, E. B.: Measurement of Picosecond Pulse Substructure Using Compression Techniques. Appl. Phys. Letters 14, 112-114, February 1969.

7. Treacy, E. B.: Optical Pulse Compression with Diffraction Gratings. IEEE J. Quant. Elect. QE-5, 454-458, September 1969.

8. Gabor, D.: Theory of Communication. J. Inst. Elect. Eng. Part III, 93, 429-457, 1946.

9. Koenig, W., H. K. Dunn and L. Y. Lacy: The Sound Spectrograph. J. Acous. Soc. Am., 18, 19-49, July 1946. The experimental techniques have become refined over the years, and many references are to be found in the J. Acous. Soc. Am. for example.

10. Shimizu, F.: Frequency Broadening in Liquids by a Short Pulse. Phys. Rev. Letters 19, 1097-1100, November 1967.

11. Gabor, D.: Acoustical Quanta and the Theory of Hearing. Nature, 159, 591-594, May 1947.

12. See for example M. Abramowitz and I. A. Stegun (Editors) Handbook of Mathematical Functions, N.B.S. Applied Mathematics Series 55 U. S. Government Printing Office, Washington. The Airy function is often expressed in terms of Bessel functions of order ± 1/3, as in Reference 13.

13. Morse, P. M. and H. Feshback: Methods of Theoretical Physics, Chapter 9, McGraw-Hill Book Company, Inc., New York (1953).

REFERENCES
(cont'd)

14. Gustafson, T. K.: (Private Communication) has noted this effect.

15. Bateman Manuscript Project, A. Erdelyi (Director): Higher Transcendental Functions. Vol. 2, McGraw-Hill Book Company, Inc., New York (1953).

16. Shapiro, S. L. and M. A. Duguay: Observation of Subpicosecond Components in the Mode-Locked Nd:Glass Laser. Phys. Letters 28A, 698-699, February 1969.

17. Duguay, M. A., J. W. Hansen and S. L. Shapiro: Study of the Nd:Glass Laser Radiation by Means of Two-Photon Fluorescence. IEEE J. Quant. Elect. (to be published).

18. Born, M. and E. Wolf: Principles of Optics, the MacMillan Company, New York, 1959. See section 8.6.

19. The minimum response time was obtained when half of the stepped mirror was apertured off.

20. A preliminary account of this work has been presented. See E. B. Treacy: Direct demonstration of picosecond pulse frequency sweep. Appl. Phys. Letters 17, 14-16 (1970).

21. McCall, S. L., and E. L. Hahn, Phys. Rev. 183, 457 (1969).

22. Hopf, F. A., and M. O. Scully, Phys. Rev. 179, 399 (1969).

23. UARL Report J920479-23, Quarterly Technical Report under Contract N00014-66-C-0344, for the period 1 March 1970 to 31 May 1970.

24. Lamb, G. L. Jr., Phys. Rev. Letters 32A, 251 (1970).

25. Berezin, Yu. A., and V. I. Karpman, JETP 24, 1049 (1967).

26. Karpman, V. I., and V. P. Sokolov, JETP 27, 839 (1968).

27. Patel, C. K. N., and R. E. Slusher, Phys. Rev. Letters 19, 1019 (1967).

REFERENCES
(cont'd)

28. Shapiro, S. L., J A. Giordmaine and K. W. Wecht, Phys. Rev. Letters 19, 1093 (1967); G. Bret and H. Weber, IEEE Jl. Quant. Elect. QE-4, 807 (1968); M. J. Coles, Optics Comm. 1, 169 (1969); M. A. Bolshov, Yu. I. Golyaev, V. S. Dneprovskii and I. I. Nurminskii, Zh.ETF 57, 346 (1969)[Translation: Soviet Phys. JETP 30, 190 (1970)]; R. L. Carman, M. E. Mack, F. Shimizu and N. Bloembergen, Phys. Rev. Letters 23, 1327 (1969); M. E. Mack, R. L. Carman, J. Reintjes and N. Bloembergen, Appl. Phys. Letters 16, 209 (1970), M. J. Colles, G. E. Walrafen and K. W. Wecht, Chem. Phys. Letters (to be published).

29. Akhmanov, S. A., Mat. Res. Bull. 4, 455 (1969); Wang, C. S., Phys. Rev. 182, 482 (1969); S. A. Akhmanov, A. P. Sakhorukov and A. S. Chirkin, Zh. ETF 55, 143 (1969)[Translation: Soviet Phys. JETP 28, 748 (1969)]; T. I. Kuznetsova, Zh.ETF 10, 153 (1969)[Translation: Soviet Phys. JETP 10, 98 (1969)]; and N. M. Kroll and P. L. Kelley, Phys. Rev. (to be published).

30. Carman, R. L., F. Shimizu, C. S. Wang and N. Bloembergen, Phys. Rev. A2, 60 (1970).

31. Carman, R. L., M. E. Mack, F. Shimizu and N. Bloembergen, Phys. Rev. Letters 23, 1327 (1969).

32. Haken, H., and M. Paunthier, IEEE Jl. Quant. Elect 4, 454 (1968).

33. Mack, M. E., R. L. Carman, J. Reintjes and N. Bloembergen, Appl. Phys. Letters 16, 209 (1970).

34. Mack, M. E., IEEE Jl. Quant. Elect. 4, 1015 (1968).

35. Self focusing in an externally focused beam has been observed and was discussed: R. L. Carman, J. Reintjes and M. E. Mack, IEEE International Quantum Electronics Conference, Kyoto, Japan, 1970.

36. Gustafson, T. K., private communication.

37. Edgerton, H. E., and P. Y. Cathou, Rev. Sci. Instruments 27, 821 (1956).

38. Sorokin, P. P., J. R. Lankard, E. C. Hammond and V. L. Morruzzi, I.B.M. Journal 11, 130 (1967).

39. Stitch, M. L., and E. J. Woodbury, Proc. IRE 49, 1571 (1961).

40. Wagner, W. A., and B. A. Lengyel, J. Appl. Phys. 34, 2040 (1963).

REFERENCES
(cont'd)

41. Beaulieu, A. J., Appl. Phys. Letters 16, 504 (1970); and Gilbert, J., Bull. Amer. Soc. 15, 808 (1970).

42. Casper, J. V., and C. G. Pementel, Appl. Phys. Letters 5, 231 (1964).

FIGURE CAPTIONS
(Figs. 1 - 14 only)

1 The phase structure curve depicting relation between carrier frequency and time. An attempt to measure the curve would involve measuring the times that filters tuned to different frequencies would respond.

2 The linear chirp, characterized by a linear relation between carrier frequency and time.

3 A double-valued ω versus τ can be modeled by a parabolic relationship, which leads to an Airy function for Ψ. The pulse intensity is modulated by the interference between the upper and lower branches of the parabola.

4 A sinusoidal form of the double-valued ω versus τ. The quantity $\Omega\tau_2/2\pi$ is denoted by z in Fig. 5.

5 Pulse intensities for a flat 100 cm^{-1} bandwidth depicted for z=1,3, and 10. The number of cycles of beat depends on the product 2z of bandwidth and duration.

6 The TPF curve: $\int|\Psi(t)|^2|\Psi(t+\tau)|^2\,dt$ versus τ computed from the Ψ for z=10 in Fig. 5. Experimental points shown are from Shapiro and Duguay [16].

7 Double-valued ω-τ relationship with two turning points, modeled on a sinusoidal variation. Again the quantity $\Omega\tau_2/2\pi$ is denoted by z.

8 Pulse intensities for the same z values and bandwidth as for Fig. 5. The intensities show less fine structure than Fig. 5 because of the smaller beat frequencies between the different branches.

9 Part of a diffraction grating spectrometer illustrating some features of its response to a short pulse input.

10 Grating spectrometer modified for picosecond type response time. The spectrum is displayed in opposite directions in the focal plane FF' for the two opposing beams. A camera, not shown, photographs from above the fluorescence produced in the cell to provide a measure of frequency sweep rate.

11 The sausage shaped form and its inverted image represent the wave group constituting an optical pulse as it approaches the focal plane. In the hypothetical pulse illustrated the long wavelength components precede the shorter wavelengths. The fluorescence enhancement produced in the eye where the wave groups intersect gives the antisymmetrized spectrogram.

FIGURE CAPTIONS
(cont'd)

12 Top: TPF produced by a pulse intersecting itself in fluorescent dye cell. The pulse has not been dispersed by a spectrometer. Middle: TPF made from pulse that has been dispersed in the fast spectrometer. The pulse image has not been inverted as shown in Fig. 11. The spectrometer is adjusted for minimum response time using this configuration. Bottom: TPF made by the method shown in Fig. 11. The slope of the display gives the frequency sweep rate directly.

13 Summary of a set of frequency sweep rates measured for ultrashort pulses from a Nd:glass laser. The vertical bars indicate the extent of the variations from shot to shot of the laser.

14 (a) Curve I is constructed so that its slope at any point is consistent with the measurements summarized in Fig. 13. Curves II, III and IV represent the results of a pulse compression wherein group delays of 4, 7, and 10 psec/100 cm^{-1} have been introduced. (b) Pulse shapes reconstructed from the spectrum shown in the box together with the phase information contained in the upper curves.

TABLE 1

Dispersion Data

(Gases)

Material	Δk	β *	λ_0^{-2}*	$\lambda(\mu)$	$(n-1) \times 10^6$	$-\lambda\frac{\partial n}{\partial \lambda} \times 10^6$	$(n_p - 1) \times 10^6$	P(atm)	$\Delta n_p \times 10^6$
SF_6	775 cm^{-1}	21140*	279.49*	0.6943	702.3	11.4	713.7	1	
				0.7338	701.7	10.2	711.9		50+
N_2	2330 cm^{-1}	55939	187.94	0.6943	297.8	6.6	304.4	100	
				0.8284	296.8	4.6	301.4		300
NH_3	3339 cm^{-1}	42953	90.392	0.6943	373.1	17.5	390.6	86	
				0.9035	369.6	10.2	379.8		93•
NO	1877 cm^{-1}	39122	155.73	0.6943	292.7	9.1	301.8	34	
				0.7984	291.6	6.8	298.4		120
N_2O	1285 cm^{-1}	62983	126.84	0.6943	504.8	16.8	521.6	50	
				0.7624	503.4	13.8	517.2		220•
O_2	1555 cm^{-1}	37744	142.27	0.6943	269.2	8.0	277.2	100	
				0.7784	268.4	6.3	274.7		250
CO_2	1388 cm^{-1}	69049	156.63	0.6943	446.8	12.0	458.8	50	
				0.7684	445.7	9.7	455.4		200•
CO	2145 cm^{-1}	40452	123.60	0.6943	332.9	11.4	344.3	100	
				0.8157	331.3	8.2	339.5		480
CH_4	2914 cm^{-1}	55739*	129.15*	0.6943	438.6	14.3	452.9	100	
				0.8705	436.1	9.0	445.1		780
C_2H_4	1342 cm^{-1}	59995•	86.701*	0.6943	708.9	34.8	743.7	55	
				0.7657	705.9	28.4	734.3		520•
C_3H_6	2924 cm^{-1}	96798*	94.925*	0.6943	1042.5	46.6	1089.1	[illegible]	
				0.8712	1034.1	29.1	1063.2		235
H_2	4160 cm^{-1}	18800	137.88	0.6943	138.4	4.2	142.6	100	
				0.9763	137.4	2.1	137.5		310
HCl	2886 cm^{-1}	51583	118.49	0.6943	433.1	15.8	458.9	42	
				0.8663	430.3	10.0	450.3		360•
HBr	2558 cm^{-1}	57162	96.316	0.6943	606.6	26.7	633.3	22	
				0.8941	601.3	15.8	617.1		360•
Cl_2	556 cm^{-1}	81257	106.993	0.6943	774.5	30.6	805.1	5.6	24•
				0.7222	773.3	28.2	801.5		

(Liquids)

Material	Δk	a#	b#	λ_0^{2}#	d#	$\lambda(\mu)$	-	$-\lambda\frac{\partial n}{\partial \lambda}$	n_p	$\Delta n_p \times 10^6$
CS_2	656 cm^{-1}	2.57515	0.041695	0.0473193	0.0003	0.6943	1.61584	0.06591	1.68175	
(T = 18°C)						0.7274	1.61293	0.05902	1.67195	9800
C_6H_6	991 cm^{-1}	2.194	0.02409	0.01714		0.6943	1.49860	0.03585	1.53445	
(T = 20°C)						0.7456	1.49623	0.03083	1.52706	7400
	3064 cm^{-1}					0.8819	1.49187	0.02171	1.51358	21000
H_2O	3651 cm^{-1}	1.76148	0.0054438	0.01325862	0.01414	0.6943	1.33003	0.01565	1.34568	
(T = 20°C)						0.9301	1.32573	0.01464	1.34037	5300

\# International Critical Table--11.

• Calculated from data in Landolt-Bornstein, I, 881.

\+ Known density change from one atm to P was used to linearly extrapolate.

• Due to P being close to the liquification point, linear extrapolation yields this lower limit.

\# International Critical Tables--12-16.

TABLE II

RAMAN GAIN DATA

GAS	VIBRATIONAL						ROTATIONAL			
	$(\nu/L)_{vib}$	$(\nu/L)_{Stokes}$	$\rho^{0°C}_{1\,atm}$	$\left(\frac{\partial\alpha}{\partial R}\right)_{exp}$ ‡	$G_T^{vib}/(P\omega_L z)^{\frac{1}{2}}$	$G_T^{vib}/(\omega_L z)^{\frac{1}{2}}$ †	Re	$\alpha_o^{0°C}$	γ	γ^2
	(cm^{-1})	(cm^{-1})	(g/ℓ)	$(10^{-16}\ cm^2)$	$(atm\ J/cm)^{-\frac{1}{2}}$	$(J/cm)^{-\frac{1}{2}}$	$\left(\frac{depol.}{ratio}\right)$	$(10^{-24}\ cm^3)$	$(10^{-24}\ cm^3)$	$(10^{-48}\ cm^6)$
SF_6	775	13625	6.602					4.58		
N_2	2330	12072	1.2505	1.69	1.67×10^{-2}	1.67×10^{-1}	0.036	1.80	1.36	1.85
NH_3	3334	11066	0.77140	1.00	1.01×10^{-2}	†0.30×10^{-1}	0.011	2.21	0.9	0.81
NO	1877	12525	1.2302					1.73		
N_2O	1285	13117	1.9775				0.125	2.99	4.49	20.16
O_2	1555	12845	1.42896	1.43	1.67×10^{-2}	1.67×10^{-1}	0.065	1.59	1.64	2.69
CO_2	1388	13012	1.97693	1.83	1.94×10^{-2}	†1.48×10^{-1}	0.097	2.65	3.43	11.76
CO	2145	12255	1.2500	1.44	1.50×10^{-2}	1.50×10^{-1}	0.015	1.97	1.04	1.08
CH_4	2914	11487	0.7168	1.04	1.19×10^{-2}	1.19×10^{-1}	0.013	2.60	1.16	1.35
C_2H_4	1342	13060	1.26046				0.029	4.20	2.83	8.01
C_3H_6	2924	11478	1.9149					6.17		
H_2	4160	10242	0.08988				0.026	0.820	0.599	0.269
HCl	2886	11514	1.63911	1.00	0.76×10^{-2}	†0.45×10^{-1}	0.007	2.62	0.860	0.723
HBr	2558	11842	3.6442	1.20	0.97×10^{-2}	†0.30×10^{-1}				
Cl_2	556	13846	3.214				0.042	4.59	3.75	14.06

* ρ = density obtained from CRC

‡ Approximate since scaling should be linear in ρ not P when approaching liquification pressures

† R. R. Lippincott and G. Nagarajan, Bull. Soc. Chim. Belges 74, 551 (1965)

• UCRL Trans. No. 526

K920479-27

FIG. 1

THE PHASE STRUCTURE CURVE
(DEPICTING RELATION BETWEEN FREQUENCY AND TIME)

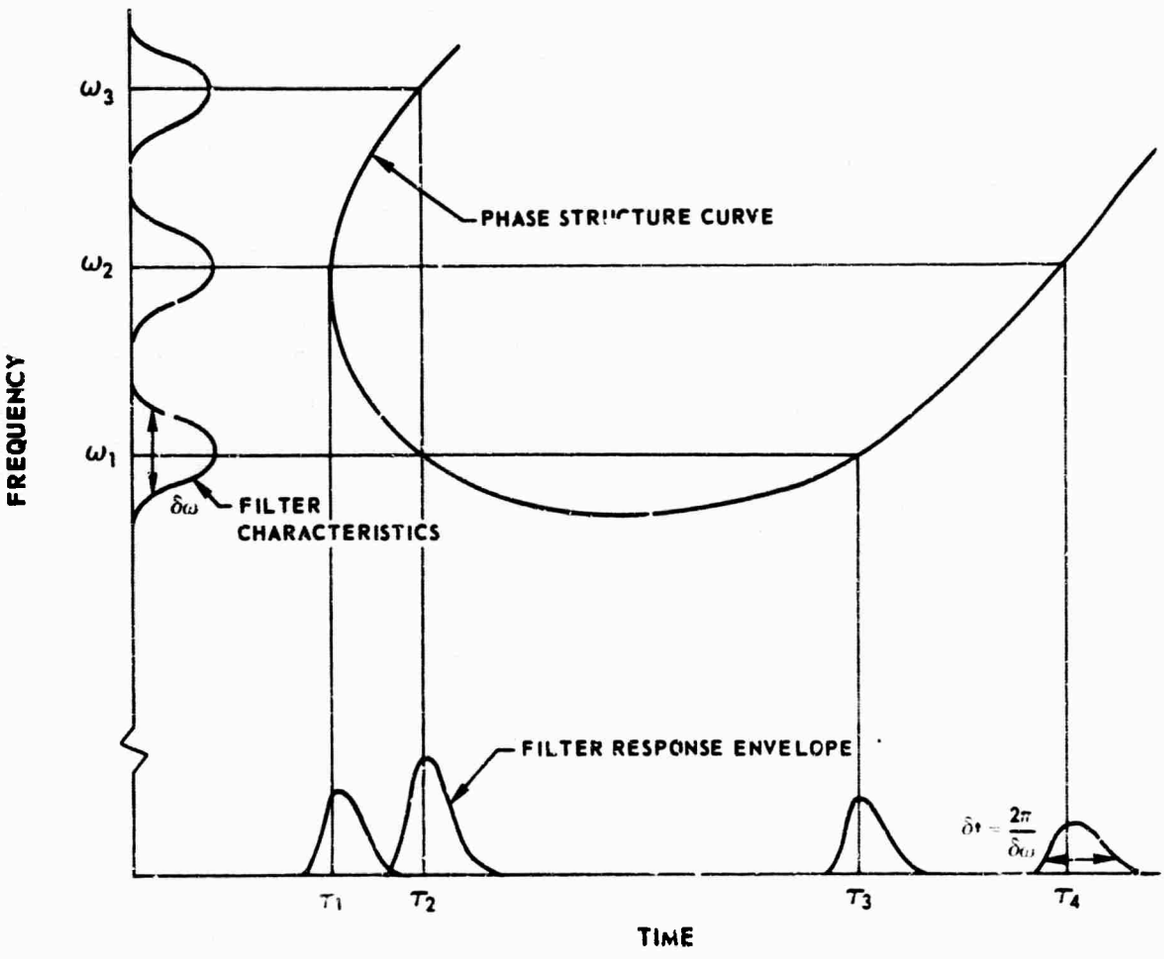

FIG. 2

LINEAR CHIRP CHARACTERISTIC

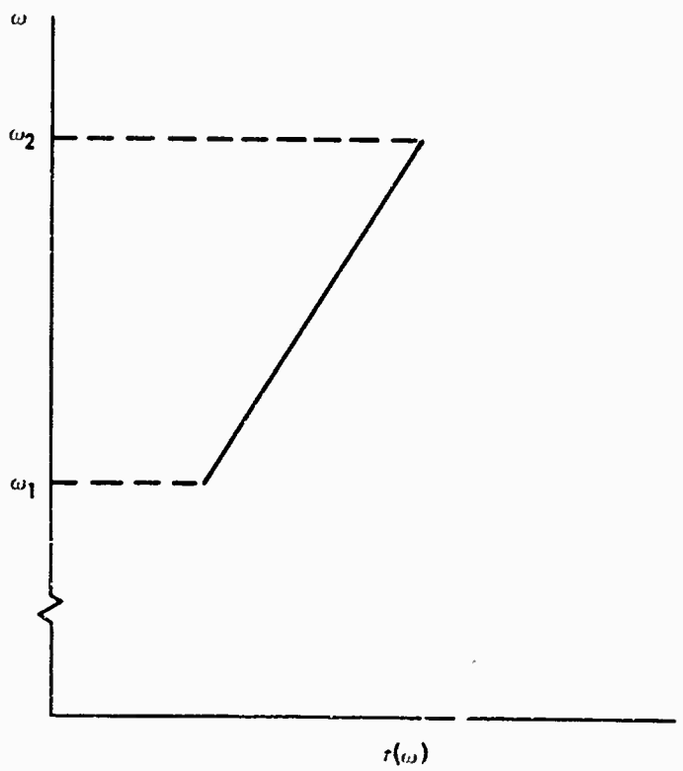

K920479-27

FIG. 3

PARABOLIC CHARACTERISTIC AND AIRY FUNCTION PULSE

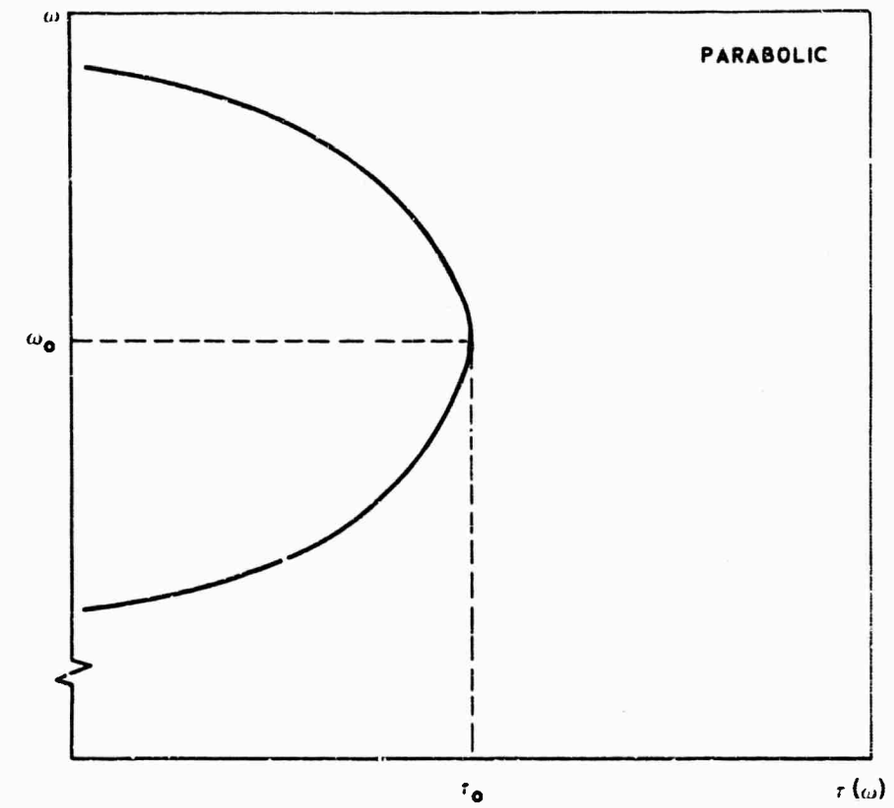

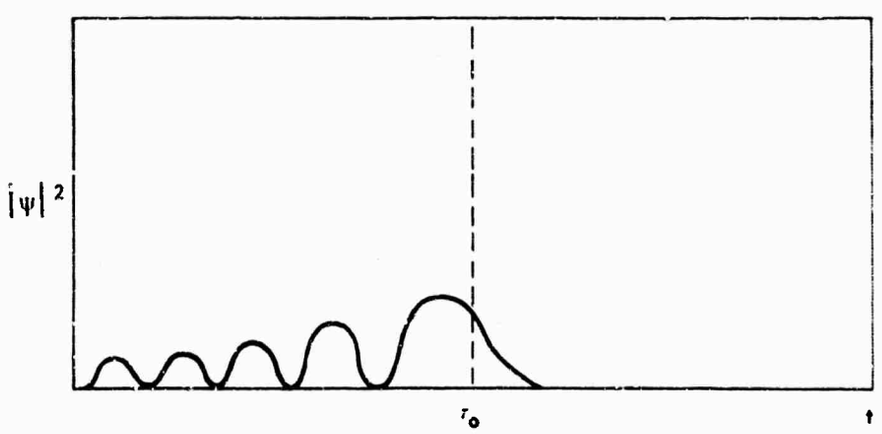

FIG. 4

SINUSOIDAL MODEL FOR DOUBLE-VALUED ω

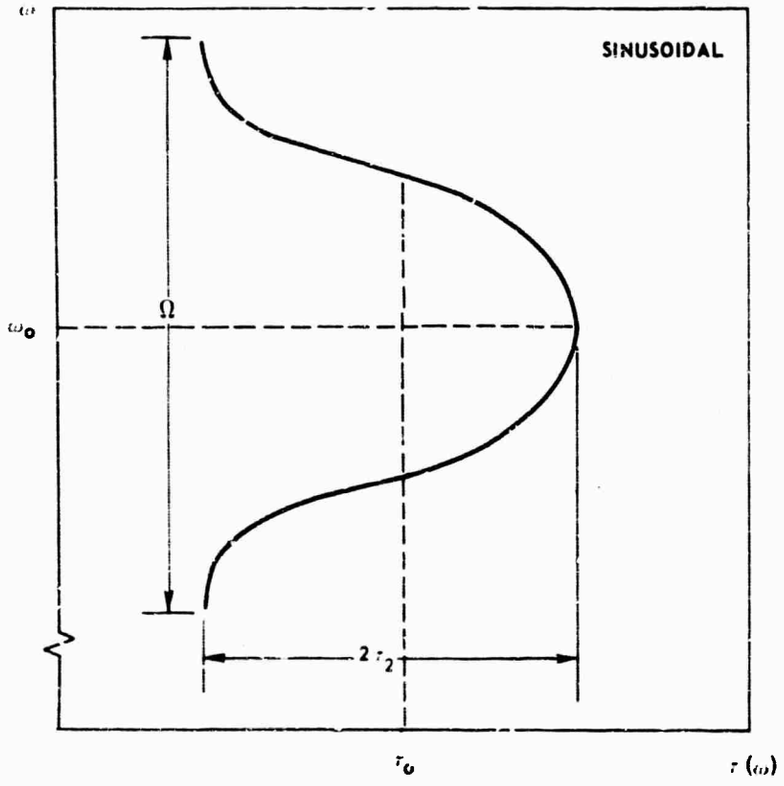

FIG. 5

ANGER FUNCTION PULSES

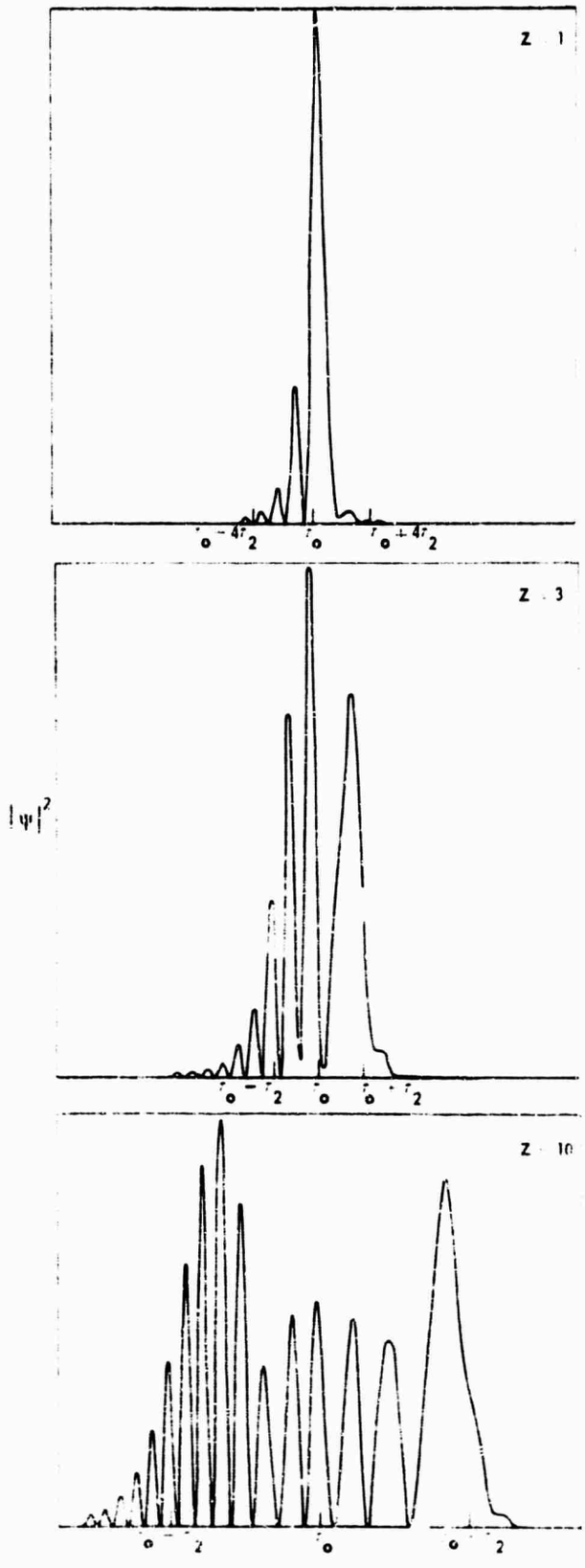

FIG. 6

TPF OF Z = 10 ANGER FUNCTION

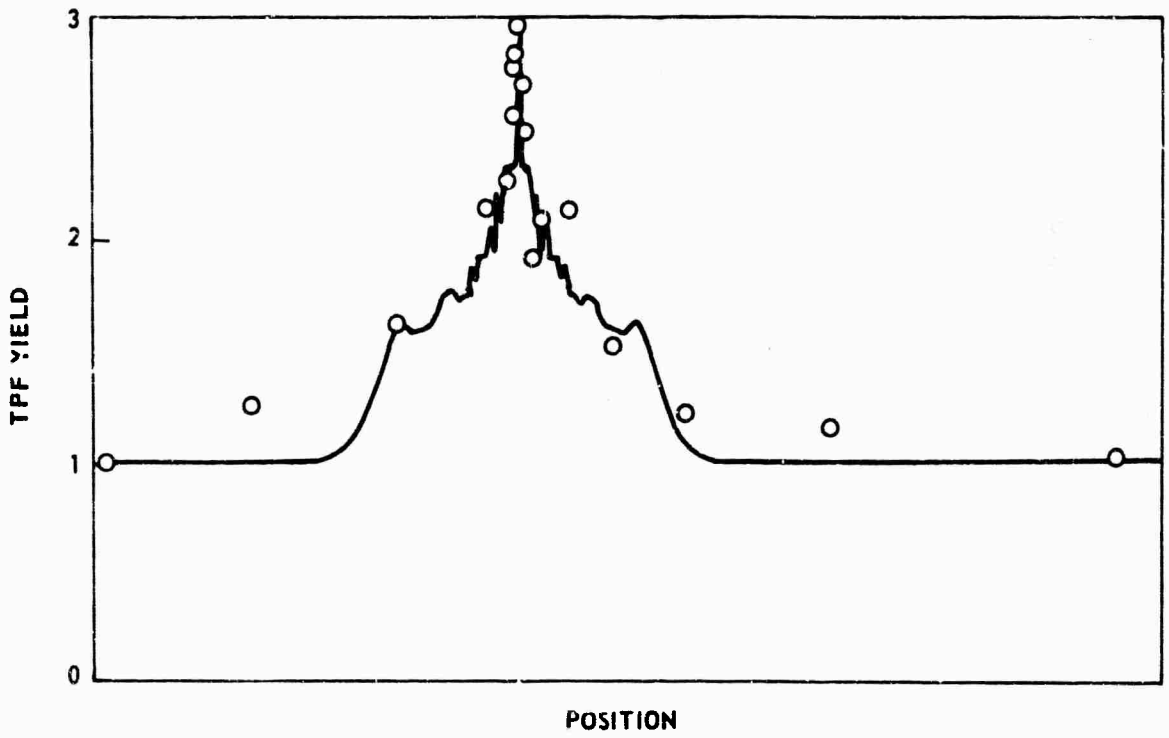

SINUSOIDAL MODEL HAVING TWO TURNING POINTS

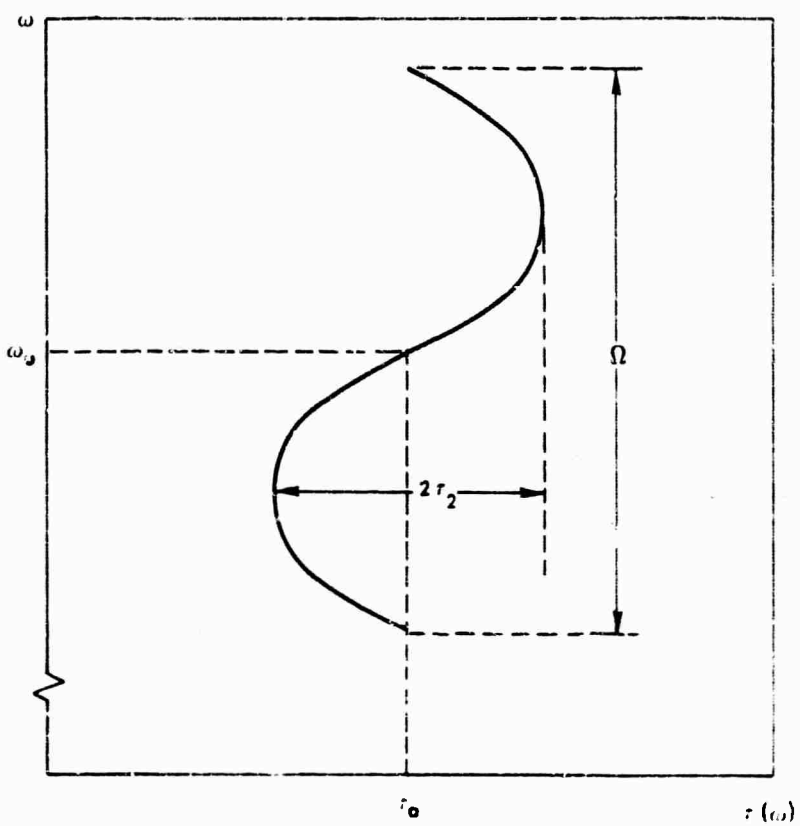

FIG. 8

PULSE FORMS FOR THE TWO TURNING POINT MODEL

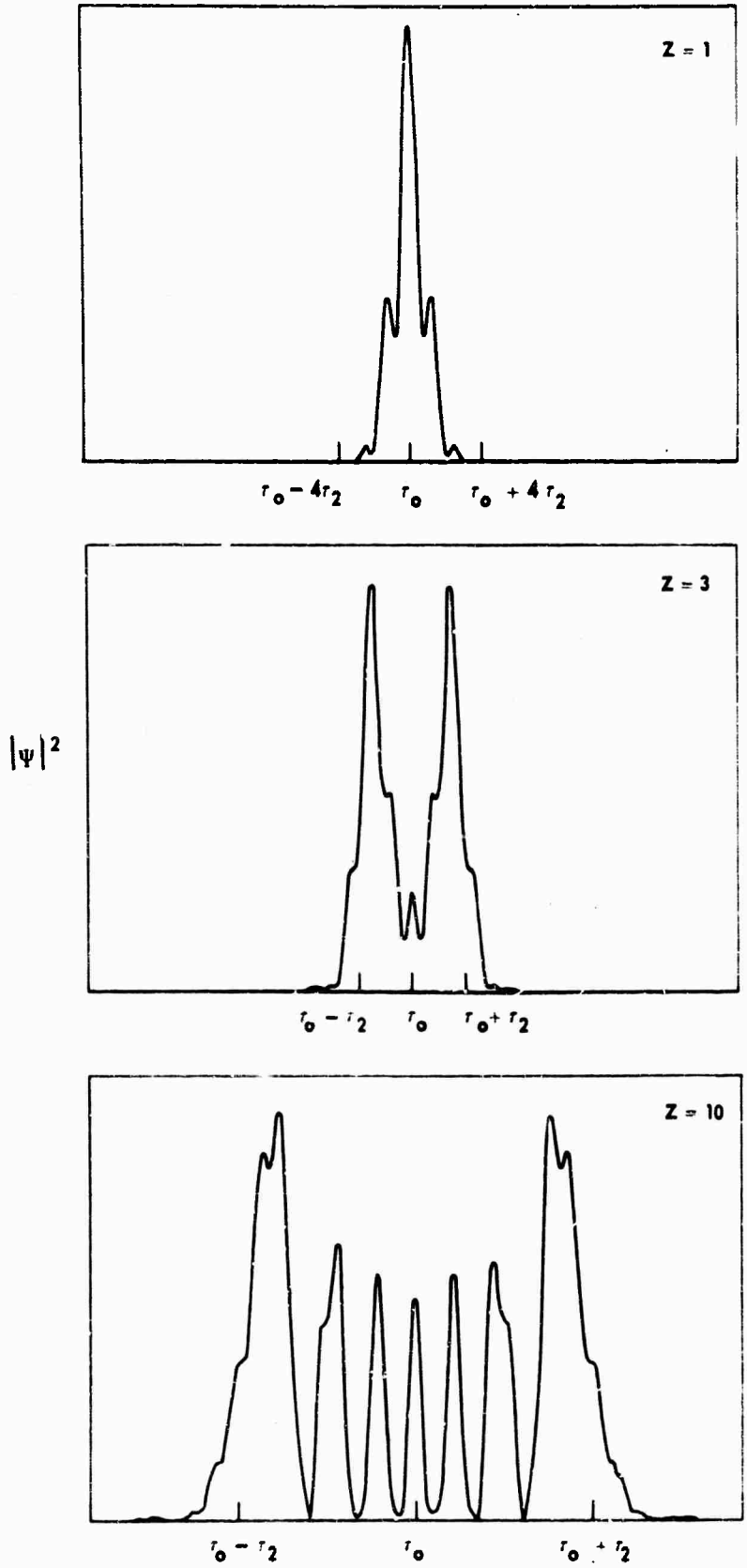

FIG. 9

GRATING SPECTROMETER

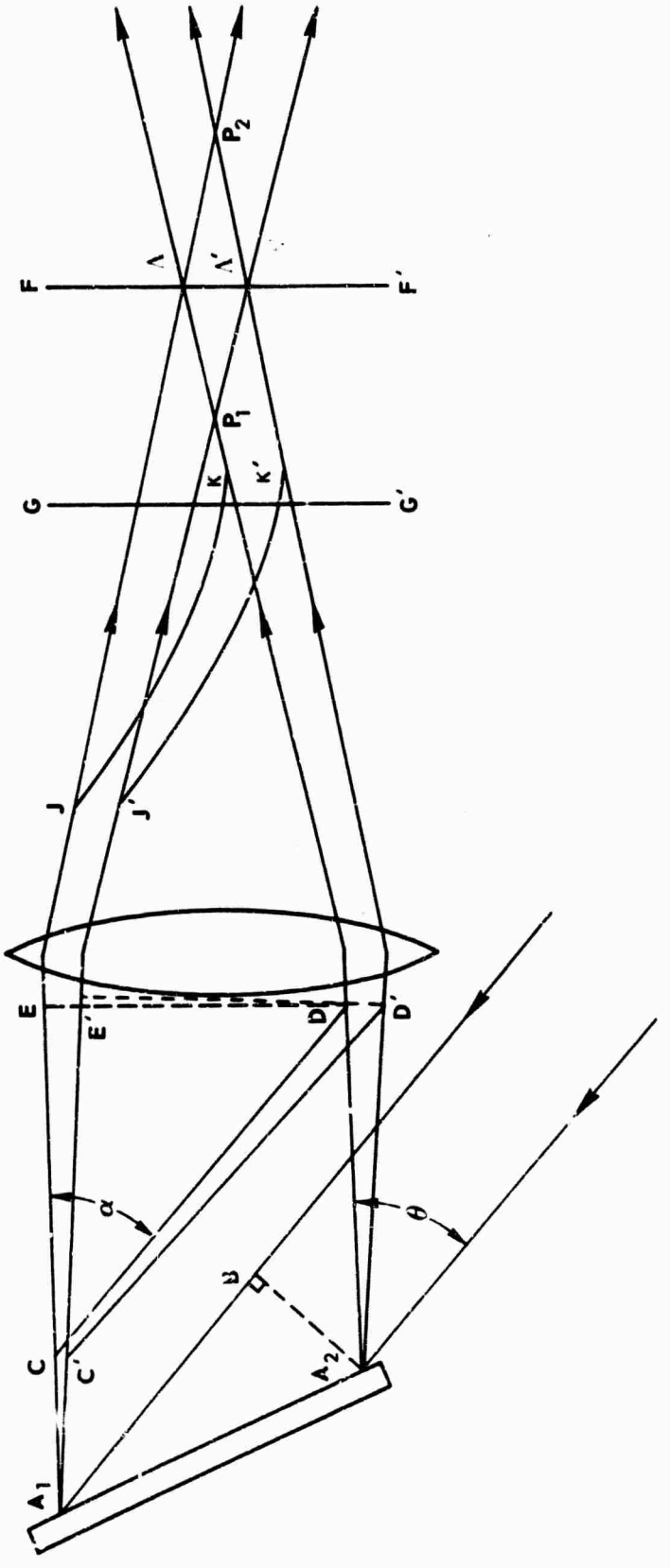

FIG. 10

APPARATUS FOR MEASURING CHIRP CHARACTERISTICS

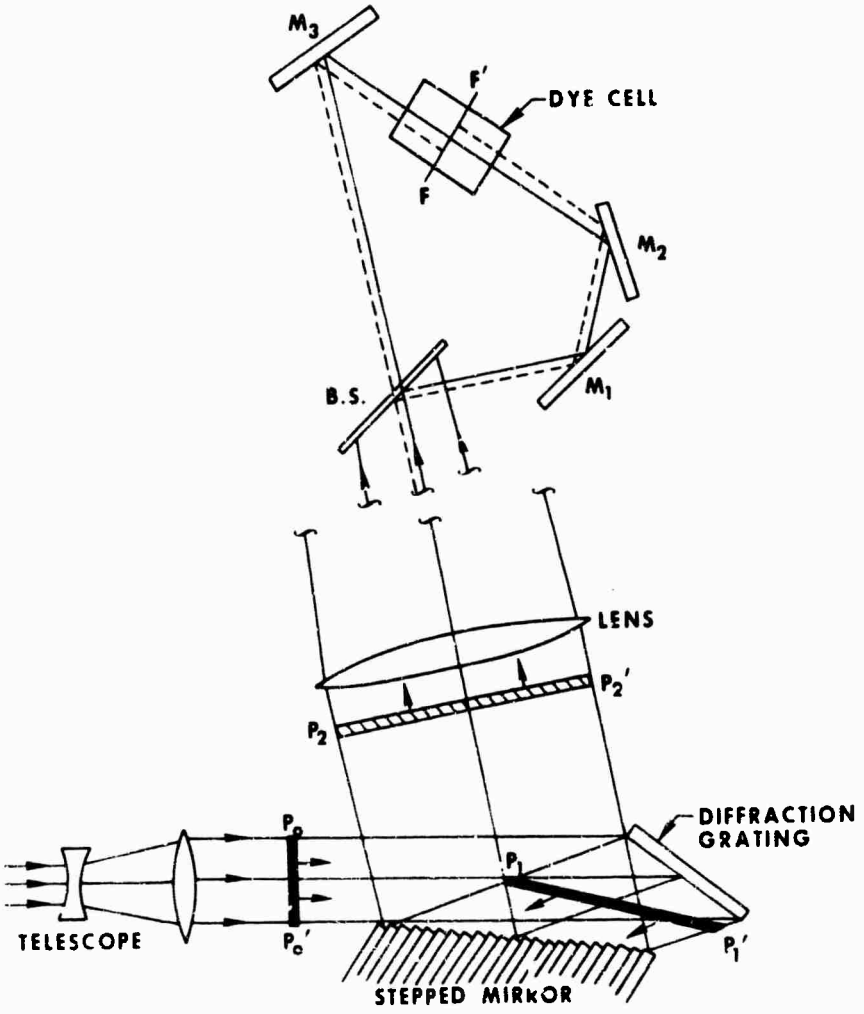

MEASUREMENT OF SLOPE AT λ′ USING TWO-PHOTON ABSORPTION-FLUORESCENCE

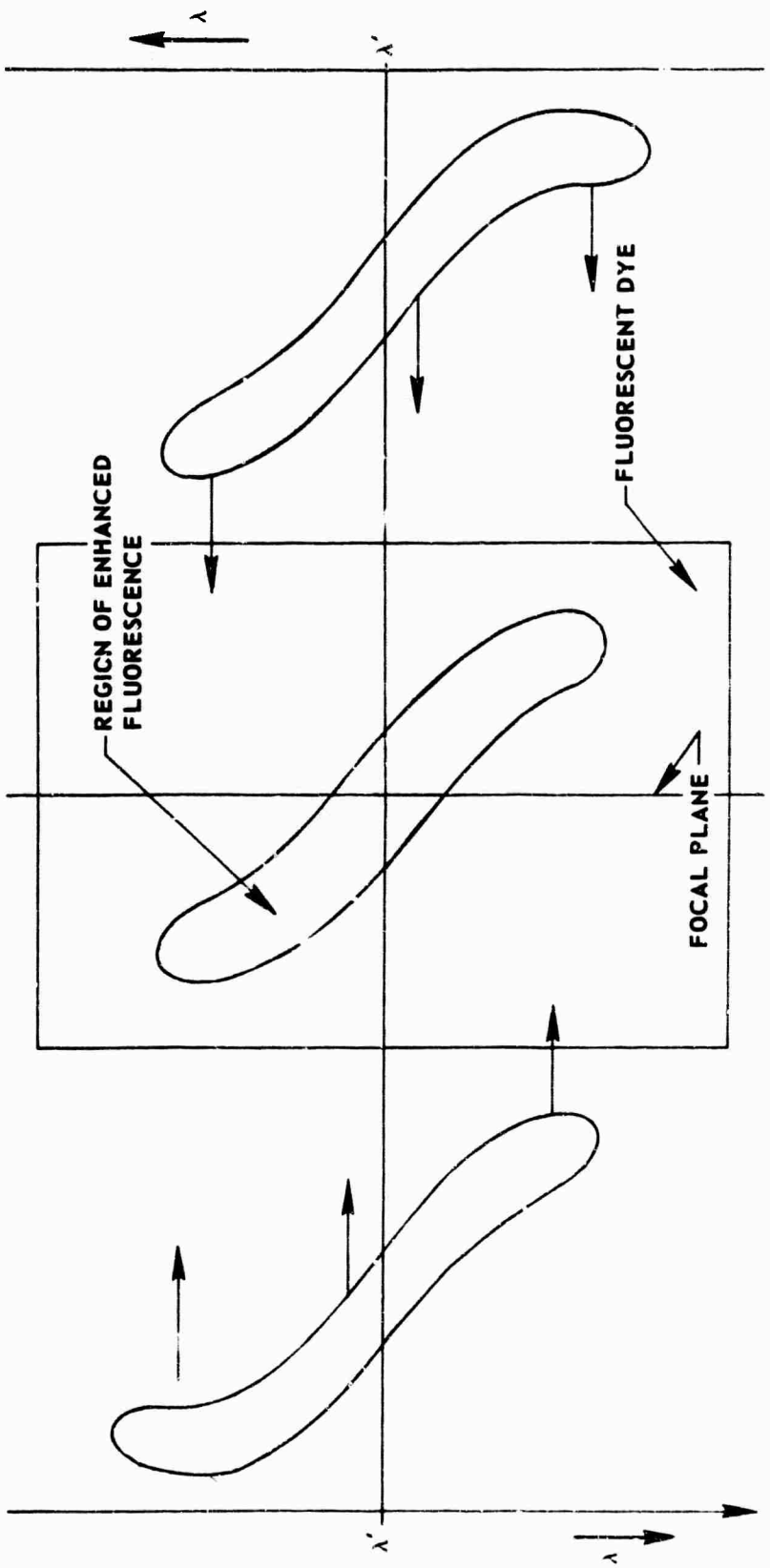

FIG. 12

COMPARISON OF THREE METHODS FOR TPF

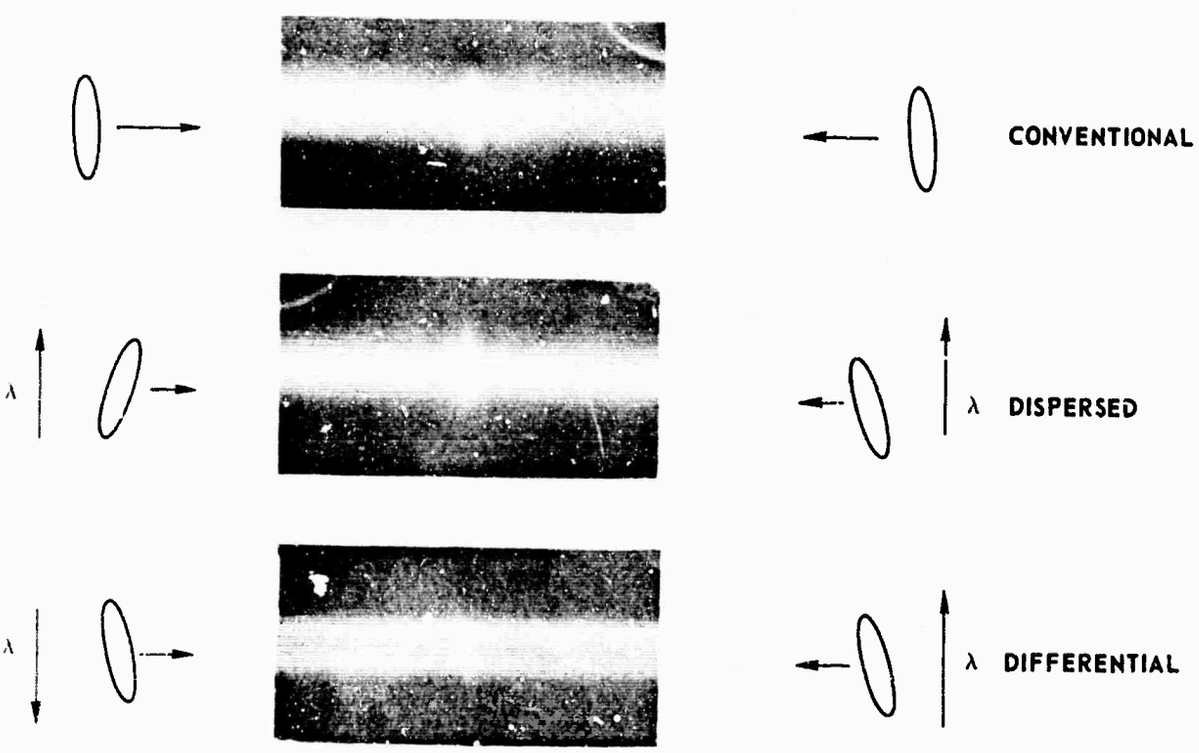

K920479-27

FIG. 13

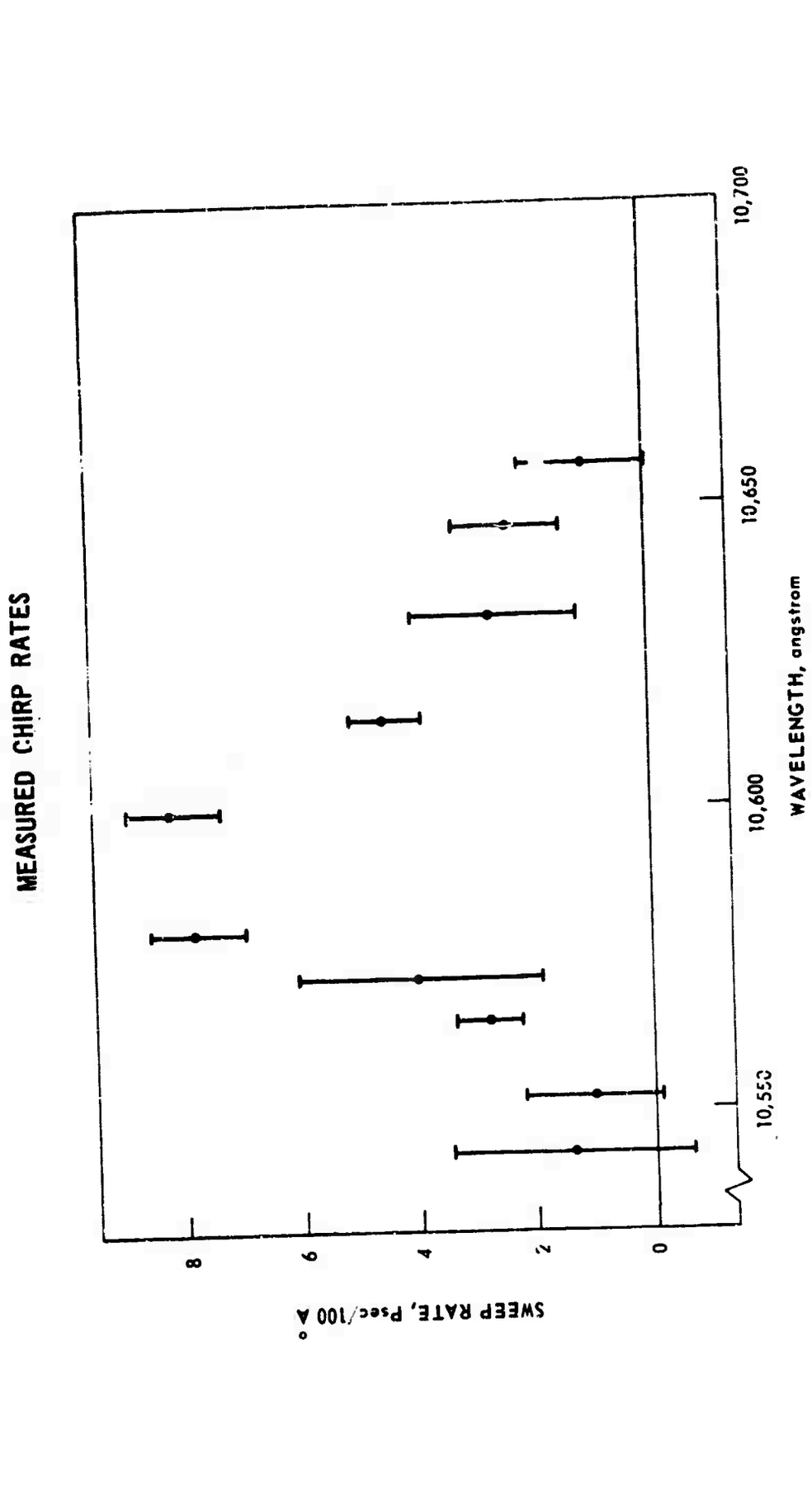

FIG. 14

EFFECT OF PULSE COMPRESSION

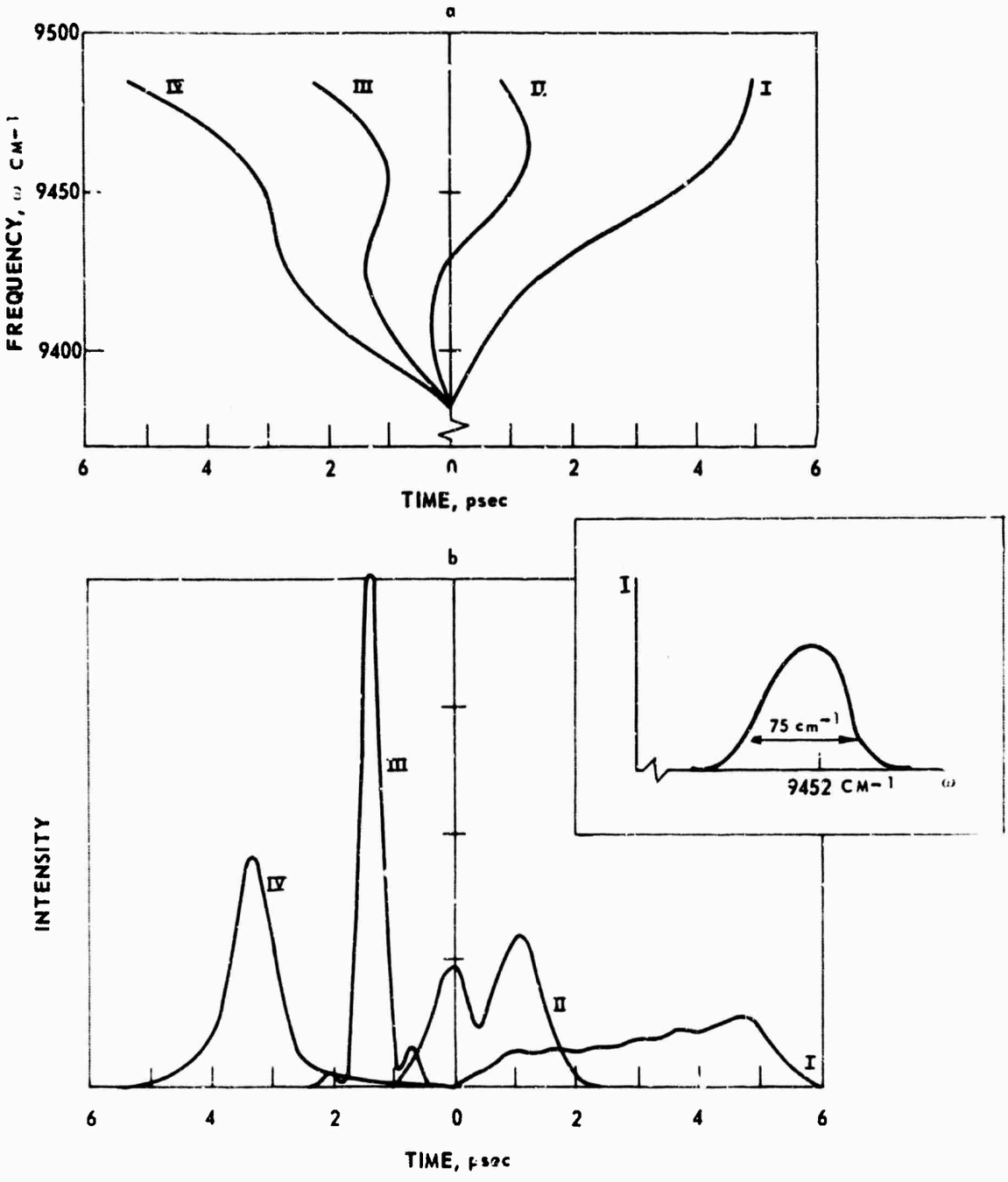

PULSE AMPLITUDES DETERMINED BY CONSERVATION LAWS

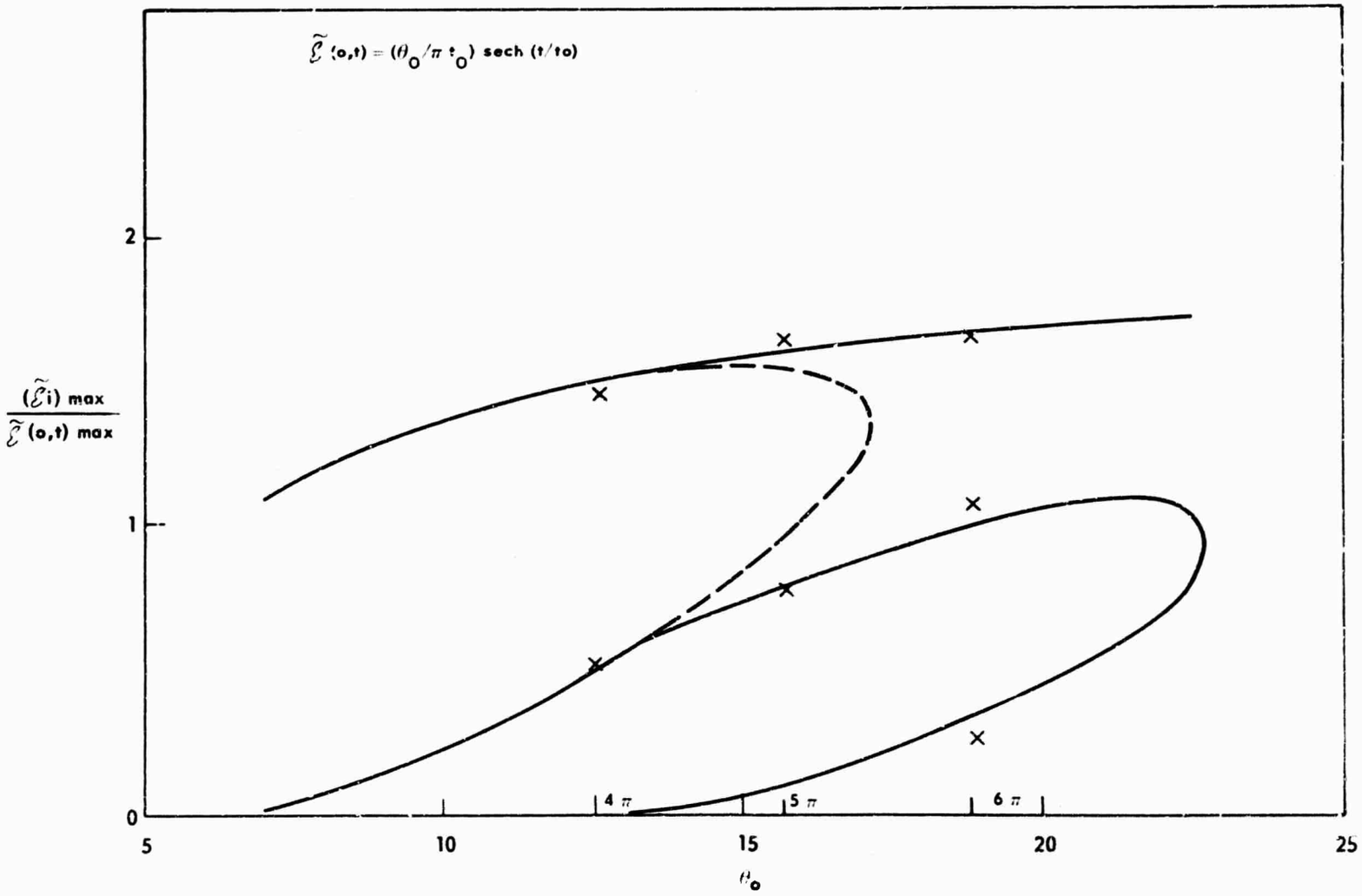

K920479-27

FIG. 16

EXPERIMENTAL ARRANGEMENT FOR OBSERVING TRANSIENT STOKES DELAY

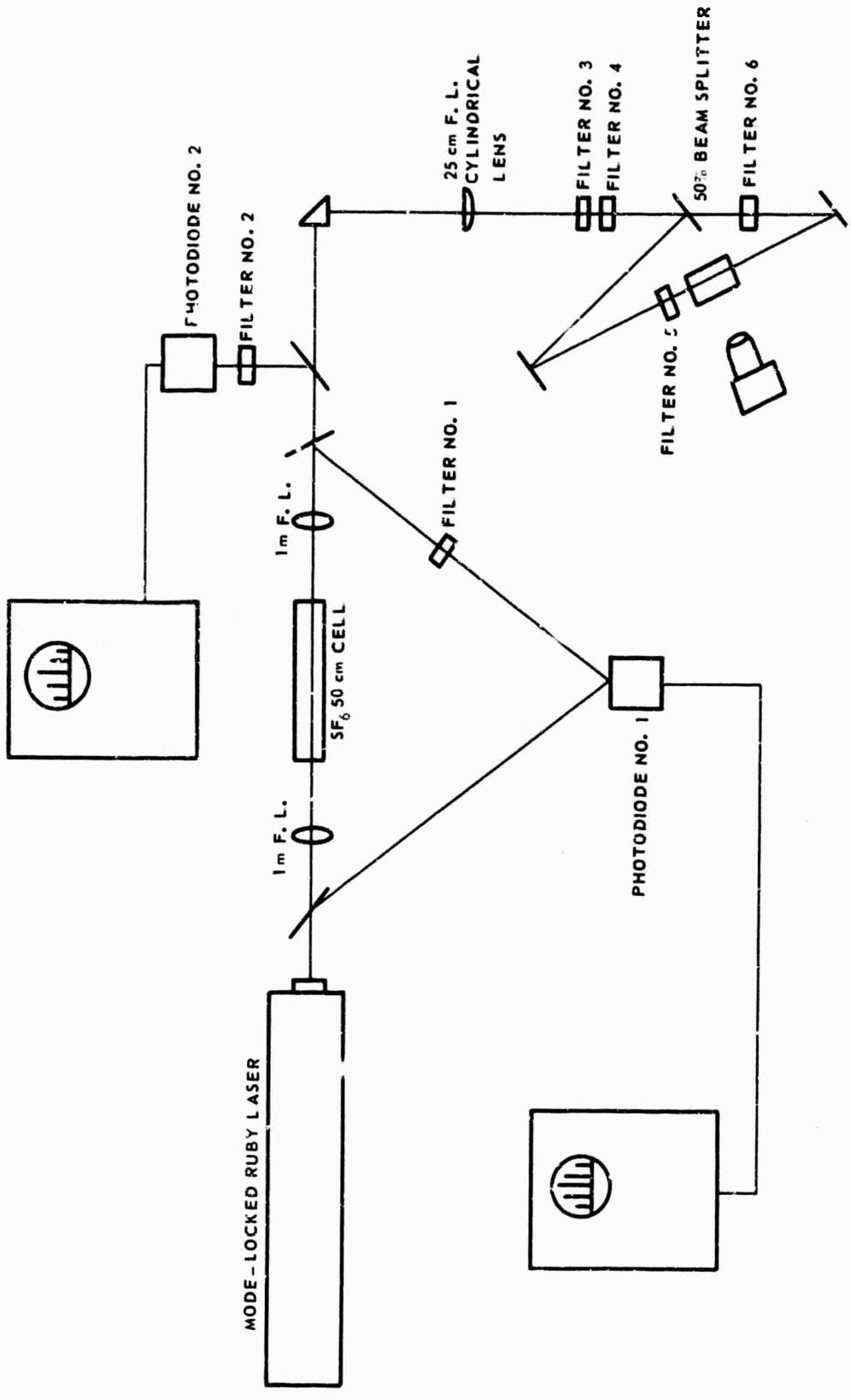

FIG. 17

STOKES GENERATION IN SF_6

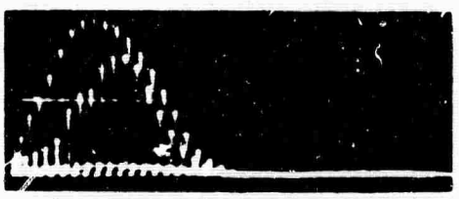

INCIDENT AND TRANSMITTED LASER

STOKES

LASER DEPLETION DUE TO STOKES CONVERSION IN SF_6

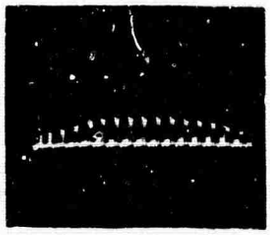

100 cm F.L.

100 cm F.L.

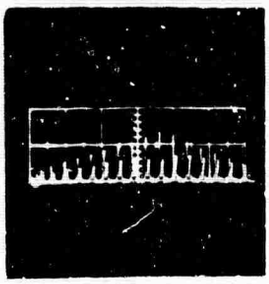

50 cm F.L.

FIG. 19

TWO PHOTON FLUORESCENCE – SF_6

LASER

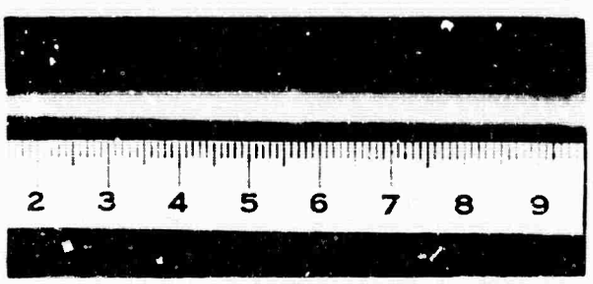

STOKES

FIG. 20

SPONTANEOUS RAMAN LINE IN SF_6

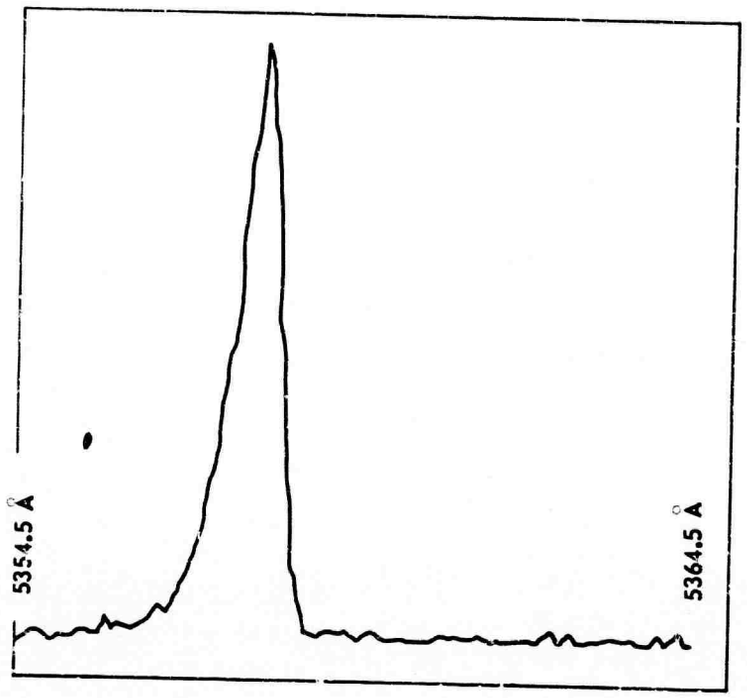

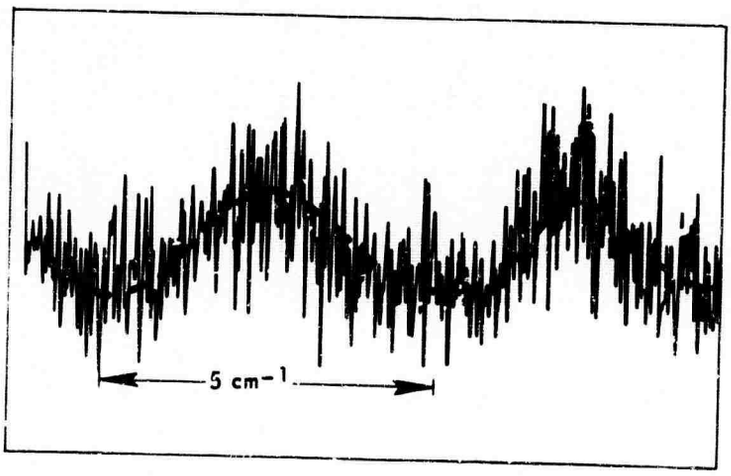

FIG. 21

RAMAN STOKES PULSE WIDTH AND DELAY - SF_6

LASER - LASER

STOKES -- STOKES

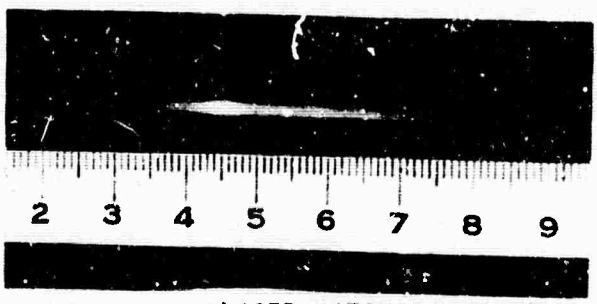

LASER - STOKES

FIG. 22

PREDICTED PROPERTIES OF TRANSIENT STIMULATED STOKES SCATTERING

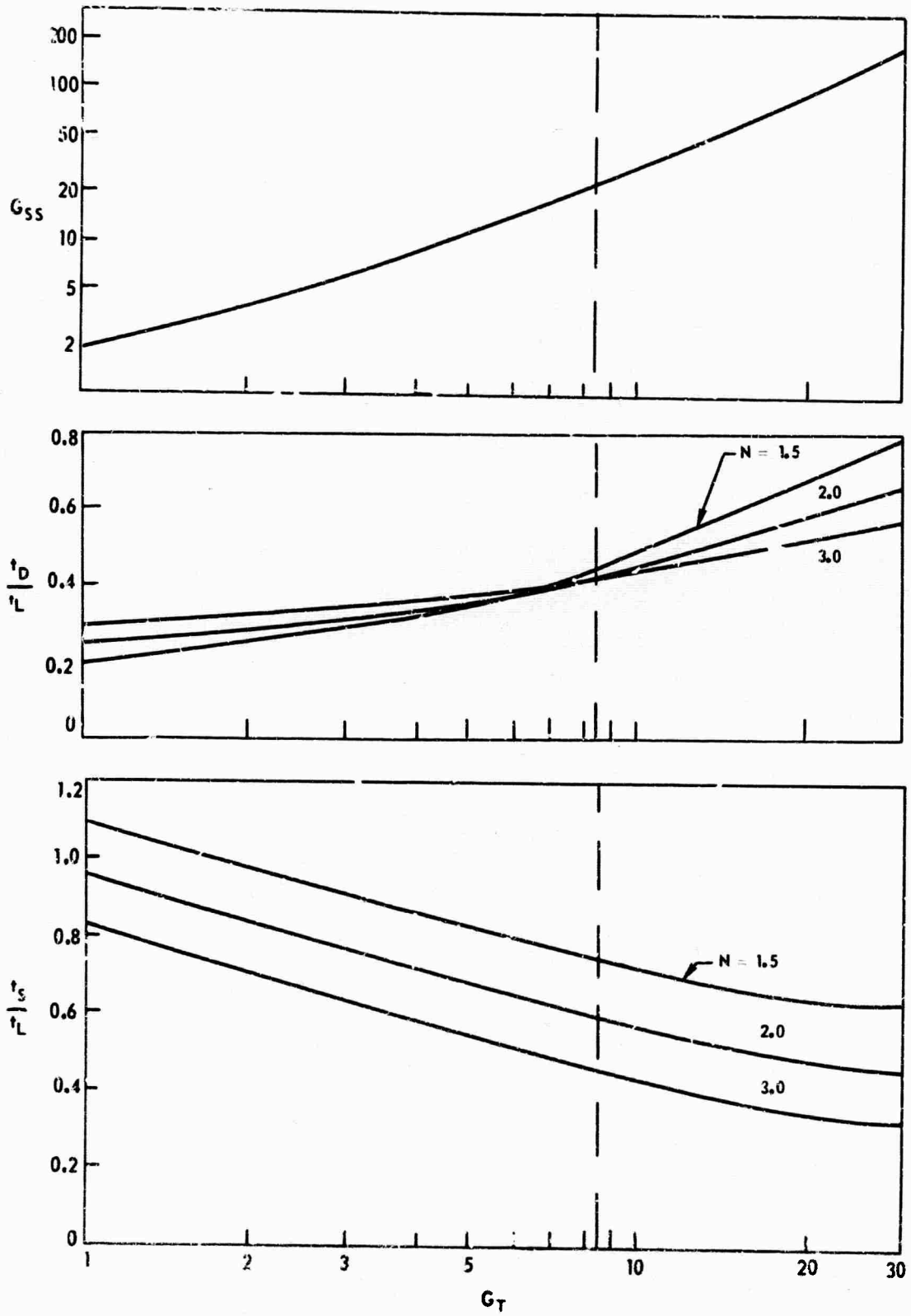

K920479-27

FIG. 23

TRANSIENT PUMPING IN DYE LASERS

20 nsec cm

A

FLASHLAMP

B

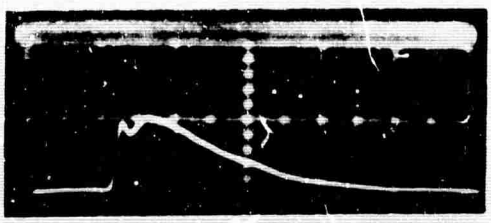

SODIUM FLUORESCEIN DYE LASER – 9 cm CAVITY

C

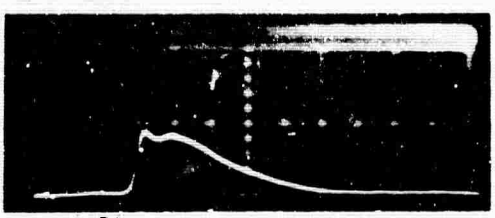

DYE LASER – 15 cm CAVITY

D

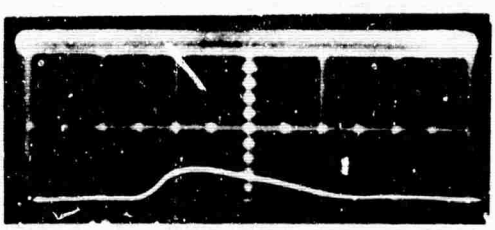

DYE LASER – 25 cm CAVITY

FIG. 24

PRESSURE AND GAP FOR 200 nsec DELAY WITH 30 kV

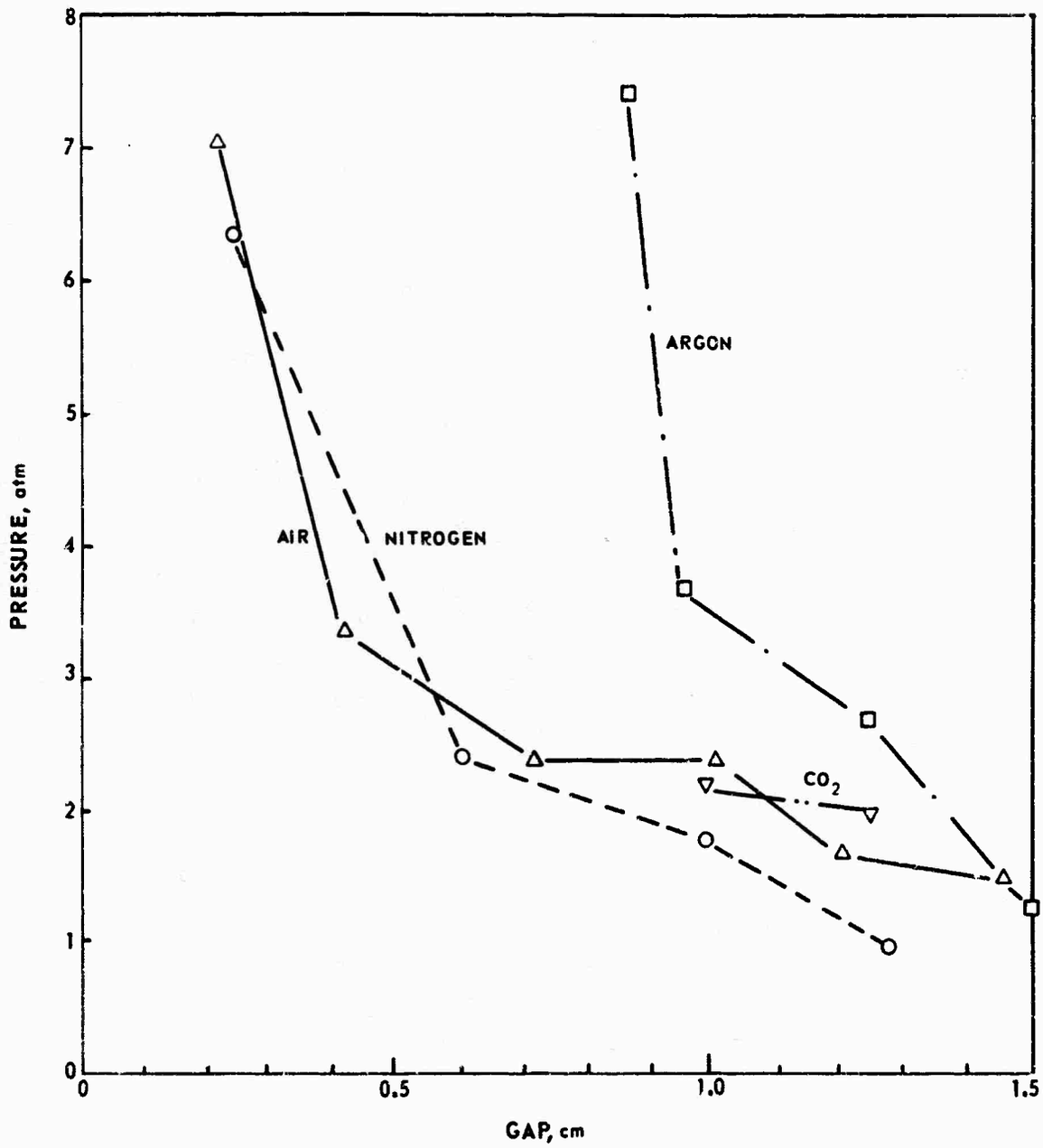

FIG. 25

UNCONFINED ARC LAMP

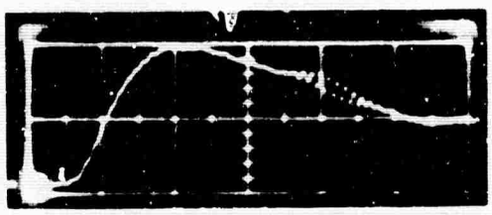

NITROGEN – 10 nsec/cm

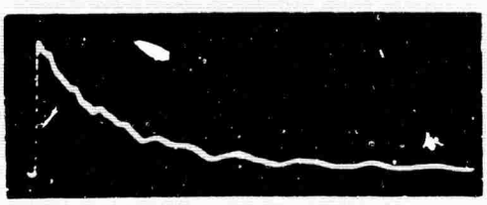

CARBON DIOXIDE – 100 nsec/cm

FIG. 26

PEAK LIGHT OUTPUT VS. GAP AND GAS

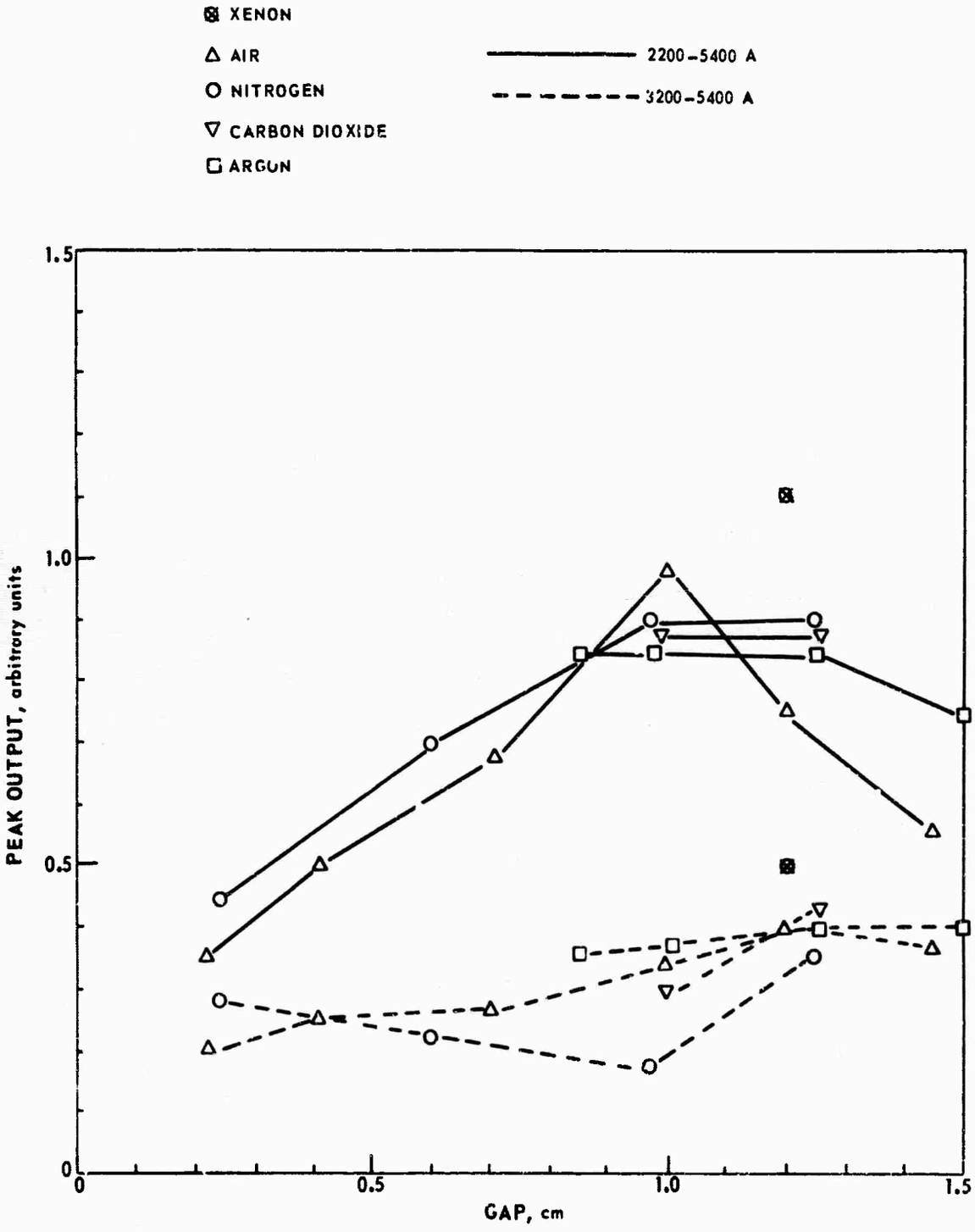

FIG. 27

OUTPUT DURATION AT 50 percent POINTS

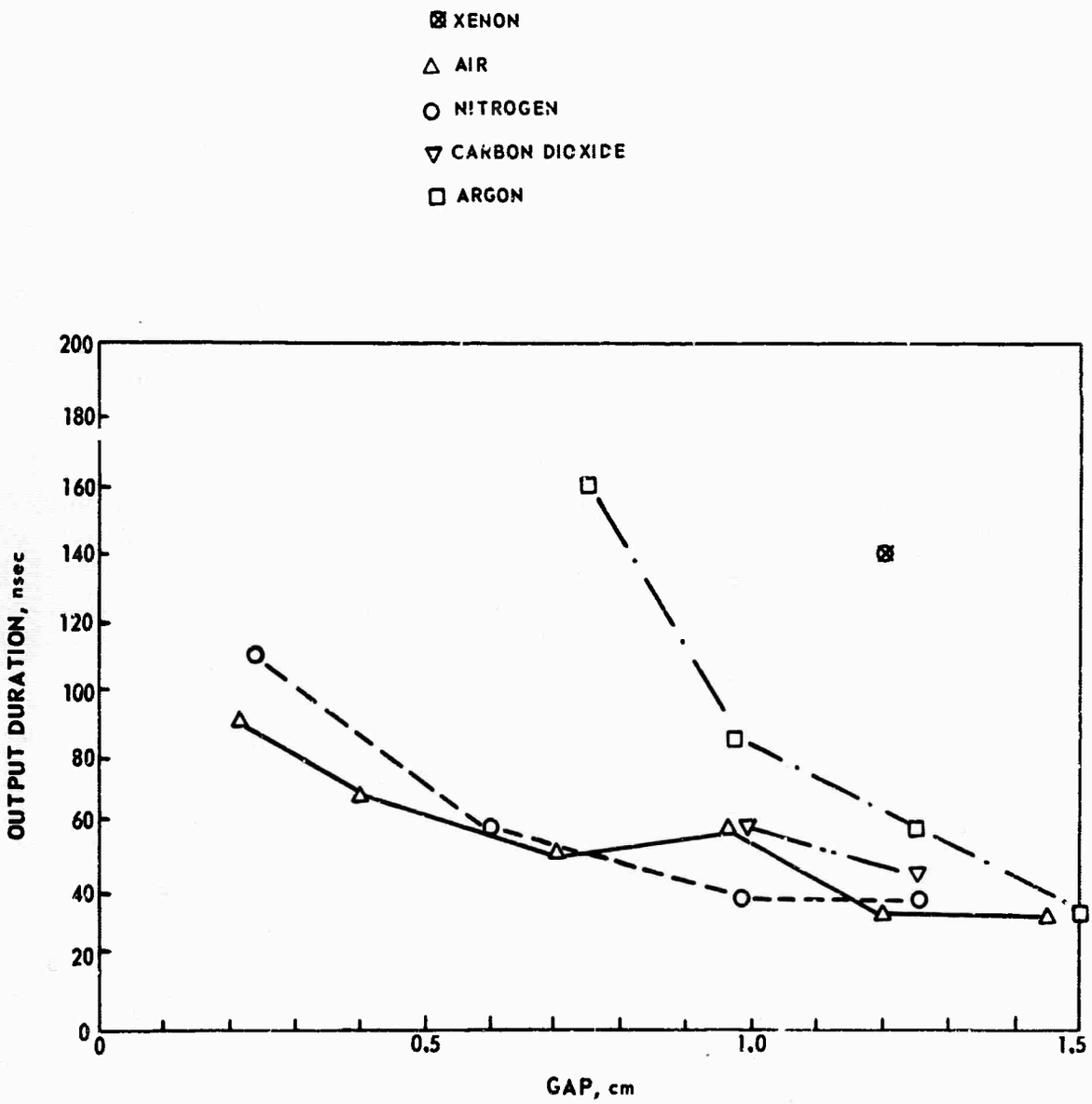

K9 20479-27

FIG. 28

INTEGRATED CAPACITOR-FLASHLAMP

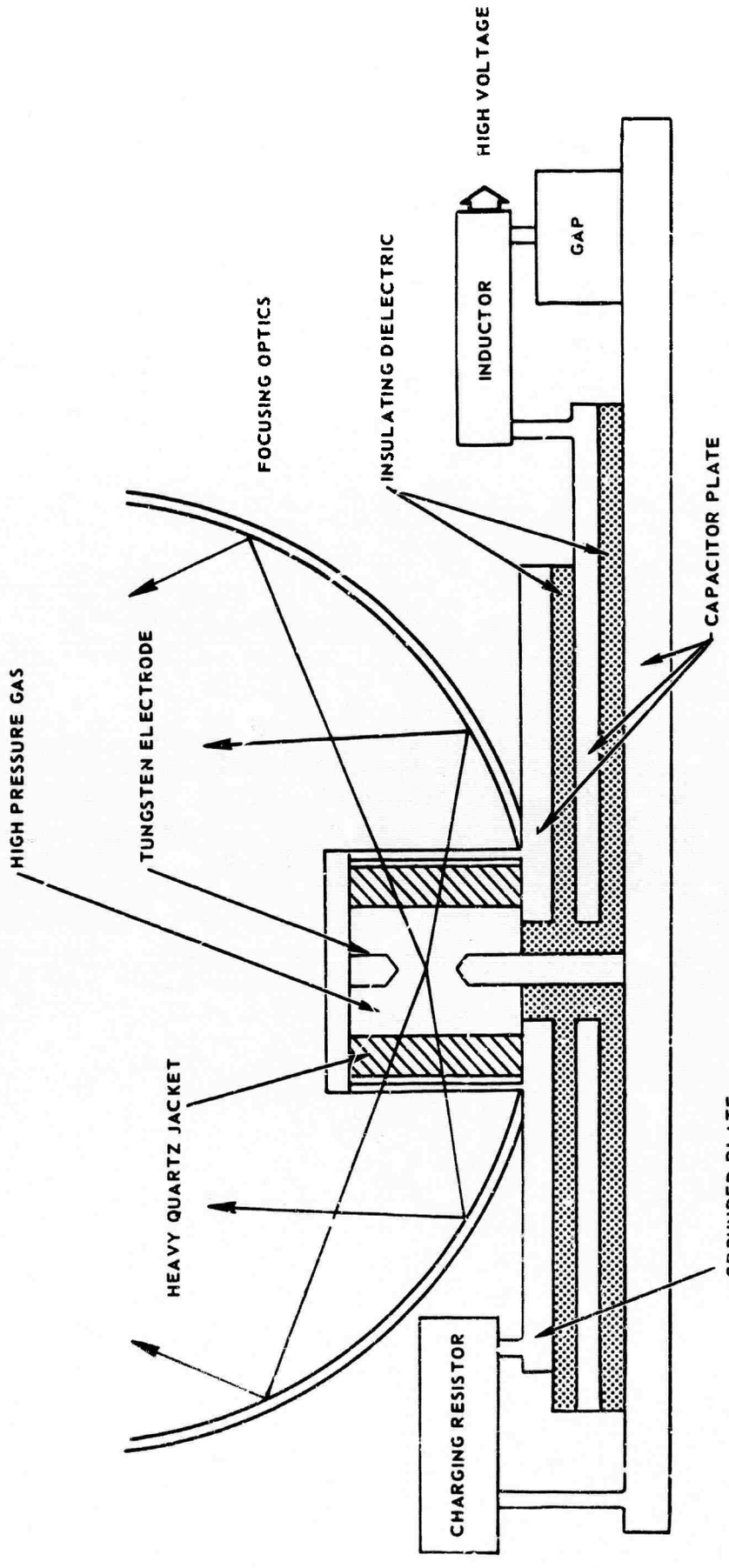

FIG. 29

DYE LASER PUMPING SCHEME